NUMERO: 2348A ANNO: 2018

A P P U N T I

STUDENTE: Corrao Stefano

MATERIA: Tunneling (Relazione) - Prof. Peila

a.a. 2015/2016

Tunnelling report

Politecnico di Torino

a.a. 2015/2016

© Proprietà riservata dell'autore - Digitalizzazione e distribuzione a cura del CENTRO APPUNTI - Corso Luigi Einaudi, 55 - Torino / Pagina 3 di 88

Contents

© Proprietà riservata dell'autore - Digitalizzazione e distribuzione a cura del CENTRO APPUNTI - Corso Luigi Einaudi, 55 - Torino / Pagina 5 di 88

1 Preliminary geological section

The aim of this first exercise is to make a preliminary geological section of specific place where the contracting authority wants to realize a 4 m diameter tunnel in order to carry water from a lode: the workplace is located near the so called *Piana dei Greci*, near Palermo (Italy).
Thanks to material provided from the contracting authority, that is a geologic map of the area and the related sections, the designer is able to find out the geological profile of the area and there is the possibility to choose between two different ways of constructing the tunnel.

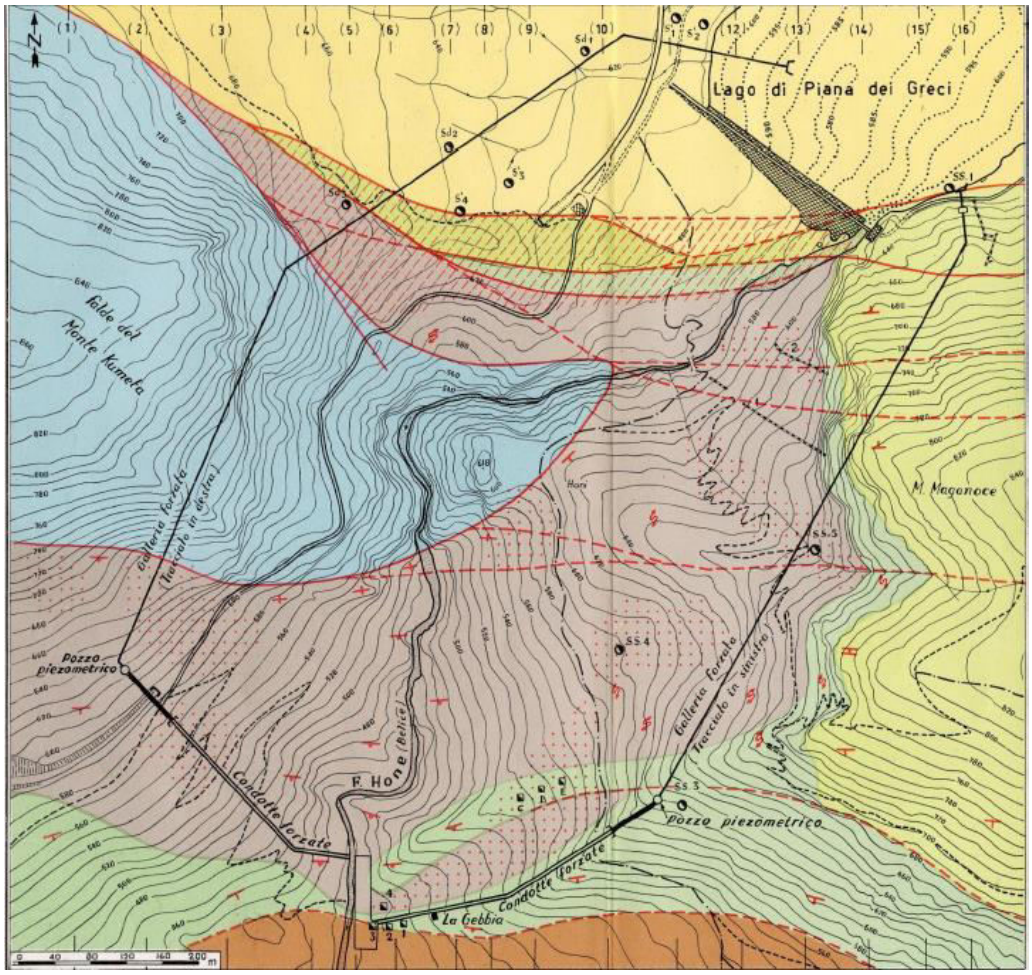

Figure 1.1: planimetry.

The choice has been made considering what is not only the most economical situation but also the less risky and so the realization of the tunnel has been made on the Eastern slope: the tunnel is about 830 m long and it carries water from an altitude of 610 meters above sea level to 580 meters above sea level.

During the definition of a tunnel design, a very important part is to choose how to construct it and which technique best fit the situation, but each of these techniques has advantages and limitations and so it's very important taking into consideration all the possible details.
Looking at the circular tunnel shape and its destination (water transport), it can be appropriate the use of a full face rock TBM. But if we consider the length of the tunnel (about 830 meters) and the almost linear morphology, mainly composed by limestone with no specific singularity (faults and not cohesive ground), the choice fell on the *Drill and blast technique.*
In addition, tunnelling by using drill and blast is often preferable to TBM or road header tunnelling if, for example, the tunnel is relatively short so that the high investment costs needed for a tunnelling machine are not economic, or when the ground hardness is very high so that a high wear of the cutter tools leads to an uneconomic application of the machine. As with all other types, excavating using drill and blast is principally most economic when it is continuous and similar work processes are used.
Ground vibrations need to be considered when using drill and blast for the excavation of a tunnel, especially in urban areas, as these can affect surface and subsurface structures (and humans), but, as the distance from a urban area is significant, the only problem in this case is the slope stability and the interactions with the road near the workplace.

© Proprietà riservata dell'autore - Digitalizzazione e distribuzione a cura del CENTRO APPUNTI - Corso Luigi Einaudi, 55 - Torino / Pagina 9 di 88

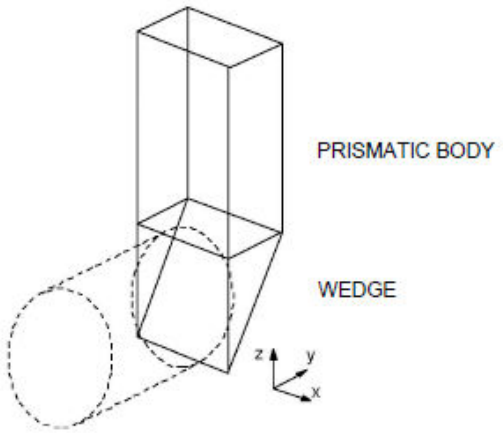

Figure 2.2: failure mechanism consisting of a wedge and a prismatic body.

As the deformation of the ground is not taken into account in a limit equilibrium analysis, only the shear strength parameters are considered, so the cohesion c and the friction angle φ (homogeneous and isotropic ground obeying Coulomb failure criterion).
The forces acting on the wedge (Figure 2.3) are:

- $G \rightarrow weight\ of\ the\ wedge$;
- $V \rightarrow vertical\ load\ resulting\ from\ the\ prismatic\ body$;
- $T/N \rightarrow shear/normal\ force\ \ applied\ at\ the\ inclined\ slip\ surface$;
- $T_s/N_s \rightarrow shear/normal\ force\ \ applied\ atthe\ lateral\ slip\ surfaces$;
- $S \rightarrow face\ support\ force$.

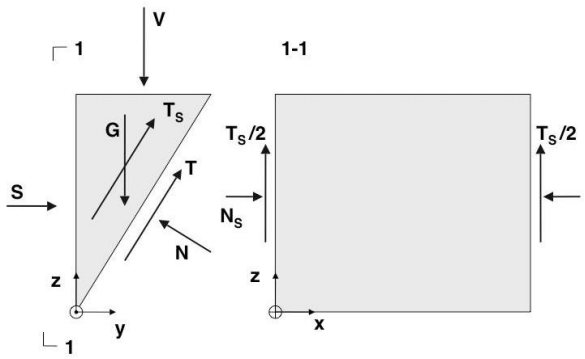

Figure 2.3: acting forces.

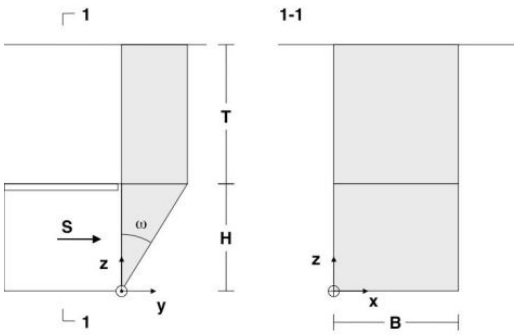

Figure 2.4: geometric parameters.

2.1 Clay

Data

- $Permeability \rightarrow k = 10^{-9}\ {}^{m}/_{s}$;
- $Weight\ of\ the\ volume\ unit \rightarrow \gamma = 19\ {}^{kN}/_{m^3}$;
- $Undrained\ shear\ strenght \rightarrow s_u = 50\ kPa$;
- $Cohesion \rightarrow c' = 5\ kPa$;
- $Friction\ angle \rightarrow \varphi' = 18°$.

Geometric parameters are:

- $Height\ of\ the\ wedge \rightarrow H = 8\ m$;
- $Width \rightarrow B = 8\ m$;
- $Depth \rightarrow T = 20\ m$.

2.1.1 Long term analysis

Using the previous equations, the results are summarized in the following table and in Figure 2.5:

ω [°]	ω [rad]	F [m^2]	U [m]	R [m]	σ_v [kPa]	V [kN]	G [kN]	T_s [kN]	S [kN]
1	0,017	1,12	16,28	0,07	-14,22	-15,89	84,90	11,57	-768,28
2	0,035	2,23	16,56	0,13	-9,37	-20,94	169,85	24,08	-548,18
3	0,052	3,35	16,84	0,20	-4,68	-15,68	254,91	37,50	-326,70
4	0,070	4,48	17,12	0,26	-0,13	-0,57	340,12	51,80	-105,47
5	0,087	5,60	17,40	0,32	4,29	24,00	425,54	66,95	114,24
6	0,105	6,73	17,68	0,38	8,57	57,66	511,23	82,92	331,48
7	0,122	7,86	17,96	0,44	12,74	100,10	597,22	99,71	545,49
8	0,140	8,99	18,25	0,49	16,79	151,04	683,59	117,29	755,71
9	0,157	10,14	18,53	0,55	20,74	210,23	770,38	135,65	961,67
10	0,175	11,28	18,82	0,60	24,59	277,46	857,65	154,78	1163,04
11	0,192	12,44	19,11	0,65	28,34	352,54	945,47	174,67	1359,52
12	0,209	13,60	19,40	0,70	32,00	435,29	1033,88	195,31	1550,89
13	0,227	14,78	19,69	0,75	35,57	525,57	1122,94	216,71	1736,96
14	0,244	15,96	19,99	0,80	39,06	623,23	1212,73	238,86	1917,56
15	0,262	17,15	20,29	0,85	42,46	728,15	1303,30	261,76	2092,58
16	0,279	18,35	20,59	0,89	45,79	840,24	1394,73	285,41	2261,89
17	0,297	19,57	20,89	0,94	49,03	959,41	1487,07	309,81	2425,40
18	0,314	20,79	21,20	0,98	52,20	1085,59	1580,41	334,97	2583,03
19	0,332	22,04	21,51	1,02	55,30	1218,75	1674,81	360,90	2734,71
20	0,349	23,29	21,82	1,07	58,33	1358,84	1770,35	387,60	2880,38
21	0,367	24,57	22,14	1,11	61,30	1505,87	1867,11	415,09	3019,98
22	0,384	25,86	22,46	1,15	64,19	1659,84	1965,18	443,38	3153,47

69	1,204	166,73	57,68	2,89	160,25	26718,27	12671,15	4246,54	-2830,32
70	1,222	175,84	59,96	2,93	161,98	28482,03	13363,73	4504,93	-3716,14
71	1,239	185,87	62,47	2,98	163,71	30428,23	14126,08	4789,77	-4713,27
72	1,257	196,97	65,24	3,02	165,44	32587,30	14969,85	5105,46	-5840,44
73	1,274	209,33	68,33	3,06	167,18	34996,81	15909,43	5457,46	-7120,80
74	1,292	223,19	71,80	3,11	168,93	37703,74	16962,78	5852,57	-8583,31
75	1,309	238,85	75,71	3,15	170,68	40767,58	18152,70	6299,42	-10264,69
76	1,326	256,69	80,17	3,20	172,44	44264,85	19508,44	6809,10	-12212,19
77	1,344	277,21	85,30	3,25	174,22	48295,61	21068,30	7396,13	-14487,63
78	1,361	301,10	91,27	3,30	176,00	52993,26	22883,32	8079,83	-17173,50
79	1,379	329,25	98,31	3,35	177,80	58539,76	25023,11	8886,58	-20382,31
80	1,396	362,96	106,74	3,40	179,61	65189,80	27585,11	9853,32	-24271,66
81	1,414	404,08	117,02	3,45	181,43	73311,33	30710,09	11033,36	-29069,24
82	1,431	455,38	129,85	3,51	183,27	83456,26	34609,16	12506,73	-35116,71
83	1,449	521,24	146,31	3,56	185,12	96491,88	39614,10	14399,13	-42951,01
84	1,466	608,92	168,23	3,62	186,99	113863,69	46277,87	16920,10	-53467,19
85	1,484	731,52	198,88	3,68	188,88	138173,62	55595,77	20446,81	-68276,52
86	1,501	915,24	244,81	3,74	190,80	174625,54	69558,44	25733,60	-90601,68
87	1,518	1221,19	321,30	3,80	192,73	235361,86	92810,65	34540,55	-127962,62
88	1,536	1832,72	474,18	3,87	194,69	356809,81	139286,74	52148,01	-202919,62
89	1,553	3666,56	932,64	3,93	196,67	721105,76	278658,37	104957,60	-428275,12

S_{max}	ω
[kN]	[°]
4432,46	41

© Proprietà riservata dell'autore - Digitalizzazione e distribuzione a cura del CENTRO APPUNTI - Corso Luigi Einaudi, 55 - Torino / Pagina 15 di 88

2.1.2 Short-term analysis

Short-term stability is analyzed based upon undrained shear strength s_u. Due to the absence of frictional resistance, the assumptions made concerning the horizontal stresses are not any more necessary and simpler expressions can be derived for the forces Ts and V.
The silo pressure σv results from the vertical equilibrium of the prismatic body by taking into account a constant shear stress s_u:

$$\sigma_v = T\gamma(1 - \frac{s_u}{R\gamma}) \quad (10)$$

Since the shear stress prevailing at the two lateral slip surfaces is also equal to the undrained shear strength s_u, the resultant shear force Ts is given by the following relation:

$$T_s = s_u H^2 tan\omega \quad (11)$$

The necessary support force S can be calculated:

$$S = BH\sigma_v + \frac{1}{2}\gamma BH^2 - s_u 2H\frac{Hsin\omega + B}{sin2\omega} \quad (12)$$

It's important to highlight that for shear strengths s_u higher than $R\gamma$, the silo pressure σ_v becomes negative (see Eq. 10). In this case, the prismatic body is stable even without support and consequently it does not exert a force on the wedge (σ_v = 0 in Eq. 12).

The results are summarized in the following table and in Figure 2.6:

ω	ω	F	U	R	σ_v	V	G	T_s	S
[°]	[rad]	[m²]	[m]	[m]	[kPa]	[kN]	[kN]	[kN]	[kN]
1	0,017	1,12	16,28	0,07	-14192,49	-15854,77	84,90	55,86	-181720,22
2	0,035	2,23	16,56	0,13	-7029,06	-15709,46	169,85	111,75	-90085,71
3	0,052	3,35	16,84	0,20	-4640,28	-15563,97	254,91	167,70	-59567,73
4	0,070	4,48	17,12	0,26	-3445,17	-15418,21	340,12	223,77	-44329,71
5	0,087	5,60	17,40	0,32	-2727,51	-15272,09	425,54	279,96	-35204,35
6	0,105	6,73	17,68	0,38	-2248,59	-15125,53	511,23	336,33	-29135,93
7	0,122	7,86	17,96	0,44	-1906,09	-14978,43	597,22	392,91	-24814,85
8	0,140	8,99	18,25	0,49	-1648,84	-14830,70	683,59	449,73	-21586,36
9	0,157	10,14	18,53	0,55	-1448,44	-14682,24	770,38	506,83	-19086,72
10	0,175	11,28	18,82	0,60	-1287,82	-14532,96	857,65	564,25	-17097,71
11	0,192	12,44	19,11	0,65	-1156,14	-14382,76	945,47	622,02	-15480,48
12	0,209	13,60	19,40	0,70	-1046,16	-14231,53	1033,88	680,18	-14142,49
13	0,227	14,78	19,69	0,75	-952,87	-14079,18	1122,94	738,78	-13019,67
14	0,244	15,96	19,99	0,80	-872,70	-13925,59	1212,73	797,85	-12066,31
15	0,262	17,15	20,29	0,85	-803,01	-13770,66	1303,30	857,44	-11248,88
16	0,279	18,35	20,59	0,89	-741,85	-13614,28	1394,73	917,59	-10542,27
17	0,297	19,57	20,89	0,94	-687,71	-13456,32	1487,07	978,34	-9927,28

61	1,065	115,46	44,86	2,57	-8,58	-990,32	8774,89	5772,95	-9283,27
62	1,082	120,37	46,09	2,61	-2,93	-352,36	9147,85	6018,32	-9671,97
63	1,100	125,61	47,40	2,65	2,62	328,92	9546,14	6280,35	-9927,85
64	1,117	131,22	48,80	2,69	8,07	1058,53	9972,68	6560,97	-10041,19
65	1,134	137,25	50,31	2,73	13,42	1842,30	10430,88	6862,42	-10203,37
66	1,152	143,75	51,94	2,77	18,69	2687,03	10924,72	7187,32	-10419,21
67	1,169	150,77	53,69	2,81	23,88	3600,69	11458,87	7538,73	-10694,42
68	1,187	158,41	55,60	2,85	28,99	4592,72	12038,82	7920,28	-11035,88
69	1,204	166,73	57,68	2,89	34,03	5674,34	12671,15	8336,29	-11451,84
70	1,222	175,84	59,96	2,93	39,01	6859,01	13363,73	8791,93	-11952,33
71	1,239	185,87	62,47	2,98	43,92	8163,03	14126,08	9293,47	-12549,54
72	1,257	196,97	65,24	3,02	48,77	9606,33	14969,85	9848,59	-13258,46
73	1,274	209,33	68,33	3,06	53,57	11213,49	15909,43	10466,73	-14097,73
74	1,292	223,19	71,80	3,11	58,31	13015,29	16962,78	11159,73	-15090,69
75	1,309	238,85	75,71	3,15	63,01	15050,66	18152,70	11942,56	-16267,04
76	1,326	256,69	80,17	3,20	67,67	17369,70	19508,44	12834,50	-17665,01
77	1,344	277,21	85,30	3,25	72,28	20037,88	21068,30	13860,72	-19334,71
78	1,361	301,10	91,27	3,30	76,86	23142,52	22883,32	15054,82	-21343,05
79	1,379	329,25	98,31	3,35	81,40	26802,69	25023,11	16462,57	-23781,37
80	1,396	362,96	106,74	3,40	85,92	31185,06	27585,11	18148,10	-26777,65
81	1,414	404,08	117,02	3,45	90,40	36530,41	30710,09	20204,00	-30516,84
82	1,431	455,38	129,85	3,51	94,86	43199,88	34609,16	22769,18	-35276,52
83	1,449	521,24	146,31	3,56	99,30	51760,96	39614,10	26061,91	-41493,00
84	1,466	608,92	168,23	3,62	103,72	63159,51	46277,87	30445,97	-49893,64
85	1,484	731,52	198,88	3,68	108,13	79098,04	55595,77	36576,17	-61787,83
86	1,501	915,24	244,81	3,74	112,52	102981,54	69558,44	45762,13	-79794,61
87	1,518	1221,19	321,30	3,80	116,90	142755,06	92810,65	61059,64	-110025,30
88	1,536	1832,72	474,18	3,87	121,27	222253,63	139286,74	91636,01	-170814,36
89	1,553	3666,56	932,64	3,93	125,64	460652,48	278658,37	183327,88	-353834,82

S_{max}	ω
[kN]	[°]
-5792,79	38

© Proprietà riservata dell'autore - Digitalizzazione e distribuzione a cura del CENTRO APPUNTI - Corso Luigi Einaudi, 55 - Torino / Pagina 19 di 88

ω	ω	F	U	R	σ_v	V	G	T_s	S
[°]	[rad]	[m^2]	[m]	[m]	[kPa]	[kN]	[kN]	[kN]	[kN]
1	0,017	1,12	16,28	0,07	2,08	2,33	75,96	14,62	87,39
2	0,035	2,23	16,56	0,13	4,10	9,15	151,98	30,09	172,87
3	0,052	3,35	16,84	0,20	6,05	20,28	228,08	46,37	256,18
4	0,070	4,48	17,12	0,26	7,93	35,51	304,32	63,45	337,06
5	0,087	5,60	17,40	0,32	9,77	54,68	380,75	81,31	415,32
6	0,105	6,73	17,68	0,38	11,55	77,66	457,41	99,91	490,79
7	0,122	7,86	17,96	0,44	13,28	104,32	534,36	119,26	563,33
8	0,140	8,99	18,25	0,49	14,96	134,54	611,63	139,33	632,83
9	0,157	10,14	18,53	0,55	16,60	168,25	689,29	160,12	699,19
10	0,175	11,28	18,82	0,60	18,20	205,34	767,38	181,63	762,31
11	0,192	12,44	19,11	0,65	19,76	245,77	845,94	203,85	822,13
12	0,209	13,60	19,40	0,70	21,28	289,48	925,05	226,78	878,56
13	0,227	14,78	19,69	0,75	22,77	336,43	1004,74	250,42	931,55
14	0,244	15,96	19,99	0,80	24,23	386,58	1085,08	274,79	981,04
15	0,262	17,15	20,29	0,85	25,65	439,92	1166,11	299,88	1026,95
16	0,279	18,35	20,59	0,89	27,05	496,44	1247,92	325,71	1069,24
17	0,297	19,57	20,89	0,94	28,42	556,15	1330,54	352,29	1107,84
18	0,314	20,79	21,20	0,98	29,77	619,06	1414,05	379,63	1142,68
19	0,332	22,04	21,51	1,02	31,09	685,18	1498,51	407,74	1173,69
20	0,349	23,29	21,82	1,07	32,39	754,55	1584,00	436,66	1200,81
21	0,367	24,57	22,14	1,11	33,67	827,21	1670,58	466,39	1223,95
22	0,384	25,86	22,46	1,15	34,93	903,21	1758,32	496,97	1243,02
23	0,401	27,17	22,79	1,19	36,17	982,62	1847,31	528,41	1257,93
24	0,419	28,49	23,12	1,23	37,39	1065,50	1937,64	560,75	1268,58
25	0,436	29,84	23,46	1,27	38,60	1151,93	2029,37	594,02	1274,86
26	**0,454**	**31,21**	**23,80**	**1,31**	**39,79**	**1242,01**	**2122,61**	**628,25**	**1276,64**
27	0,471	32,61	24,15	1,35	40,96	1335,84	2217,45	663,48	1273,78
28	0,489	34,03	24,51	1,39	42,13	1433,54	2314,00	699,75	1266,15
29	0,506	35,48	24,87	1,43	43,28	1535,22	2412,35	737,10	1253,57
30	0,524	36,95	25,24	1,46	44,41	1641,03	2512,63	775,58	1235,89
31	0,541	38,46	25,61	1,50	45,54	1751,12	2614,95	815,24	1212,89
32	0,559	39,99	26,00	1,54	46,65	1865,66	2719,43	856,14	1184,39
33	0,576	41,56	26,39	1,57	47,76	1984,84	2826,22	898,33	1150,13
34	0,593	43,17	26,79	1,61	48,85	2108,84	2935,46	941,88	1109,89
35	0,611	44,81	27,20	1,65	49,94	2237,90	3047,30	986,86	1063,38
36	0,628	46,50	27,62	1,68	51,02	2372,24	3161,91	1033,35	1010,32
37	0,646	48,23	28,06	1,72	52,09	2512,12	3279,47	1081,42	950,37
38	0,663	50,00	28,50	1,75	53,15	2657,82	3400,16	1131,16	883,18
39	0,681	51,83	28,96	1,79	54,21	2809,65	3524,18	1182,67	808,37
40	0,698	53,70	29,43	1,83	55,27	2967,94	3651,76	1236,04	725,52

© Proprietà riservata dell'autore - Digitalizzazione e distribuzione a cura del CENTRO APPUNTI - Corso Luigi Einaudi, 55 - Torino / Pagina 21 di 88

84	1,466	608,92	168,23	3,62	104,87	63860,34	41406,51	19655,64	-76759,47
85	1,484	731,52	198,88	3,68	106,32	77774,20	49743,59	23810,38	-96144,08
86	1,501	915,24	244,81	3,74	107,79	98655,12	62236,50	30042,01	-125383,09
87	1,518	1221,19	321,30	3,80	109,30	133471,25	83041,11	40427,62	-174342,04
88	1,536	1832,72	474,18	3,87	110,83	203127,10	124624,97	61198,53	-272618,93
89	1,553	3666,56	932,64	3,93	112,41	412145,52	249325,91	123511,28	-568206,63

S_{max}	ω
[kN]	[°]
1276,64	26

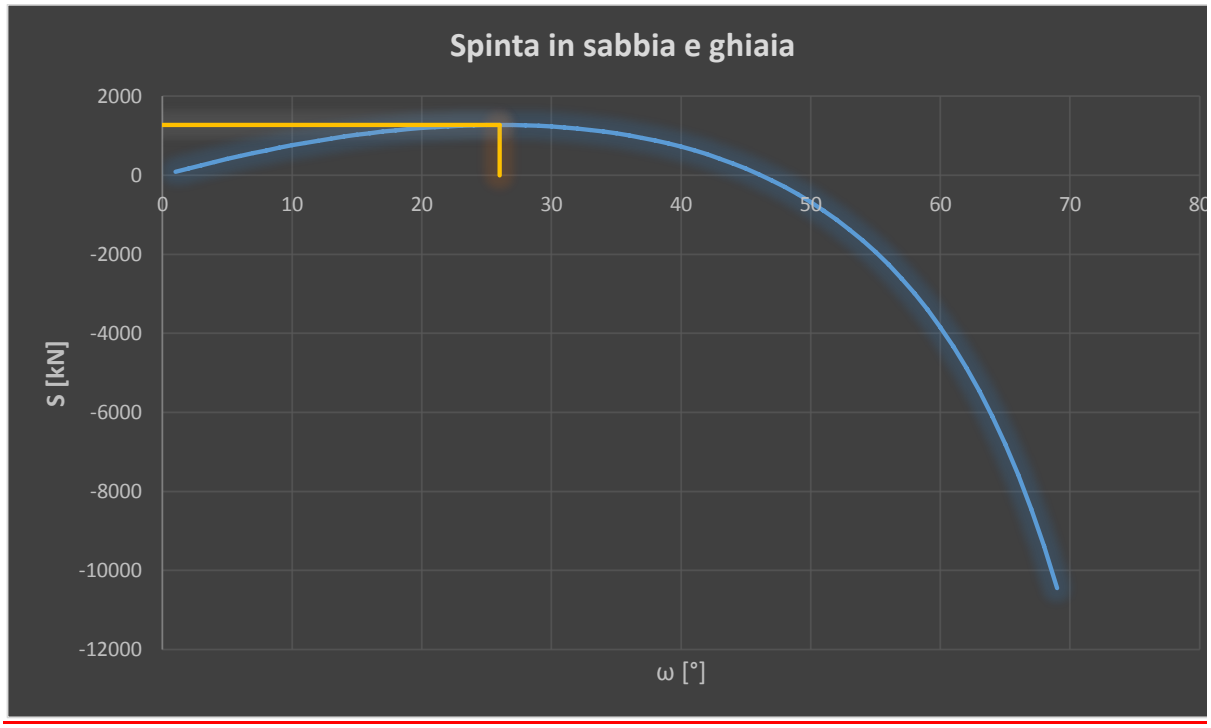

3 Production of a rock TBM

In this exercitation the aim is to determine the performance (penetration for round/wear) of a rock TBM used for the excavation of an hydraulic tunnel of 5000 m in a rock mass and mica schist. This relation must be intended as an estimated check based upon the available data for the launch of a tendering procedure made up by a company.
It must be determined:

- The penetration rate that represent the net advancement of the TBM [mm/rev];
- The wear of the cutter rings during the excavation [m^3 bench cutter];
- Net time of the excavation;
- Gross time of excavation forecasting an utilization coefficient of the 50%.

All the calculation must be developed with the Norwegian method of the NTNU.
The goal is to verify all the performance according to the hypothesis of a constant round velocity of the cutter head of 7 rpm. In order to develop all the calculation, some parameters must be known:

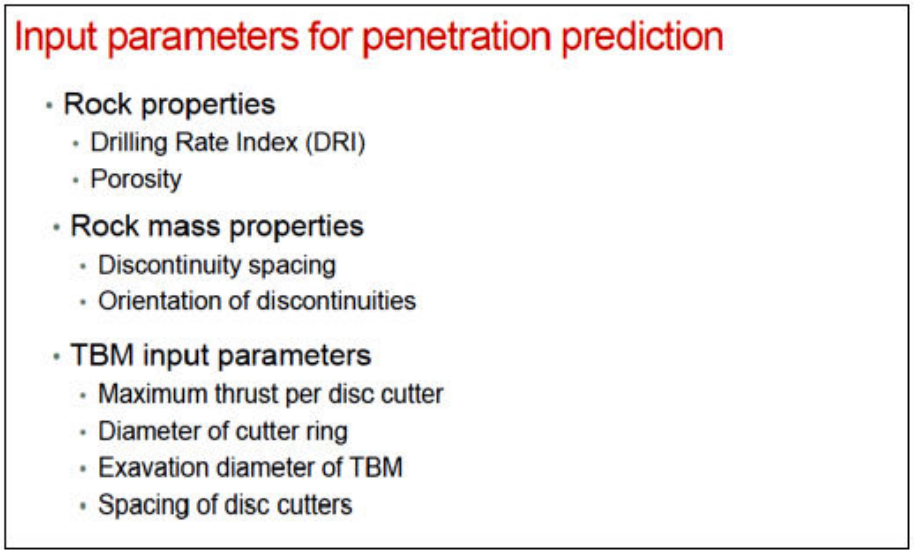

The Drilling Rate Index (DRI) is evaluated by the results of following tests, where is taken into account the average values of s_{20} and *SJ.*

© Proprietà riservata dell'autore - Digitalizzazione e distribuzione a cura del CENTRO APPUNTI - Corso Luigi Einaudi, 55 - Torino / Pagina 25 di 88

Sondaggio	CAI	S20 [%]	SJ [1/10 mm]	σ_c [Mpa]	Es [Gpa]	Et [Gpa]
1	4,1	27,16	8,6			
			5,81			
			29,6			
			1,74			
2	3,5	42,9	8,42	90	42,03	40,44
			7,28			
			0,63			
			13,4			
3	3,4	49,5	12,2	55	11,29	23,41
			8,5			
			3,95			
			7,9			
Average		39,9	9,0	72,5	26,7	31,9
DRI	**40**					

Fracture class	**III**

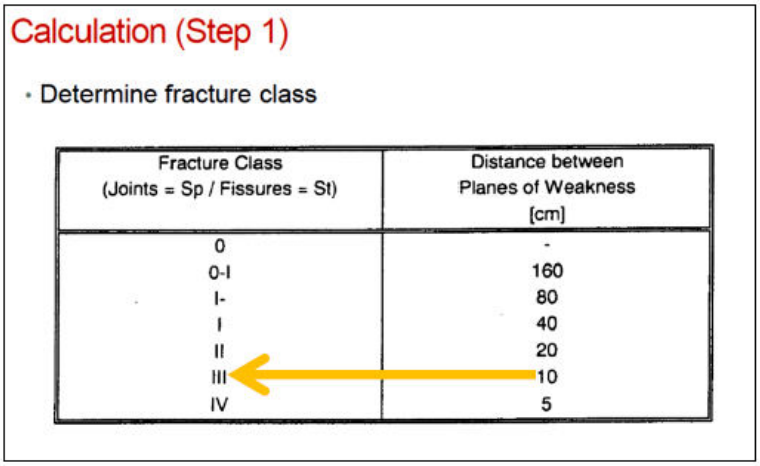

Figure 3.2: fracture class.

3.1.2 Step2:

From the geological report is known the orientation of the discontinuities (α_t - α_t) and α_f , so that in this way it is possible to calculate these parameters:

STEP 2	[°]	[rad]
α_t-α_s	5	0,087
α_f	0	0,000
α	**0**	**0,000**

STEP 3	
A [rad]	0
Fracture class	III
K_s	1,15

STEP 4	
n	1
$K_{s\text{-}tot}$	1,15

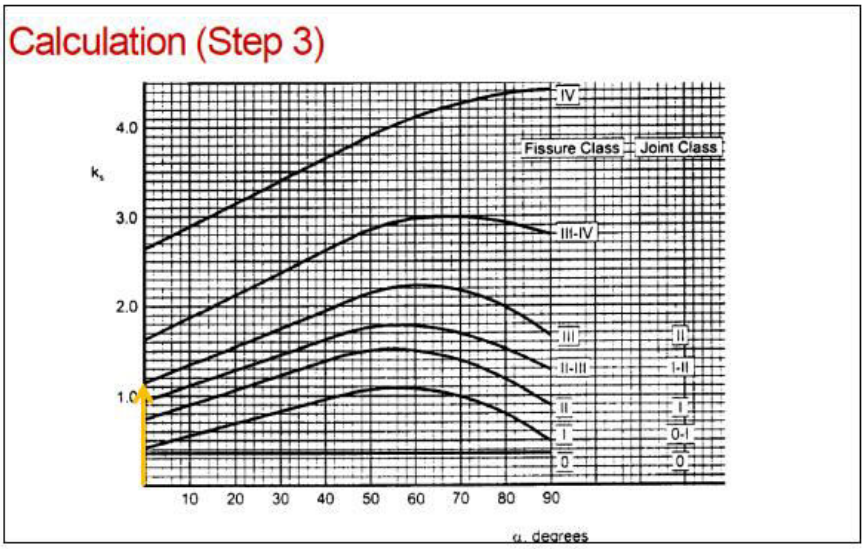

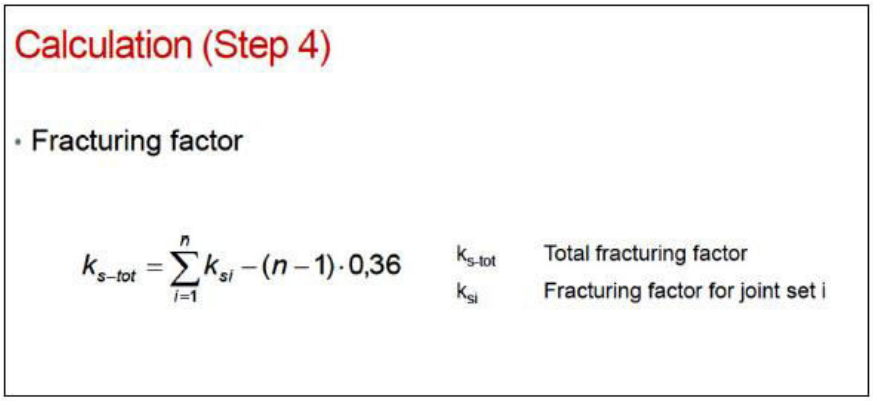

Figure 3.5: calculation of fracturing class.

3.1.4 Step 5:

Through the linear interpolation of the parameters DRI and $K_{s\text{-}tot}$, is obtained the K_{DRI}.

DRI	40

STEP 5		
K_s	K_{DRI}	
0,36	0,83	Known values
2	0,92	
1,15	0,87	Interpolated value

3.1.6 Step 7

From the average spacing of the cutter tools and the use of the following graph, is calculated K_s

STEP 7	
Average cutter spacing [mm]	70
K_a	1

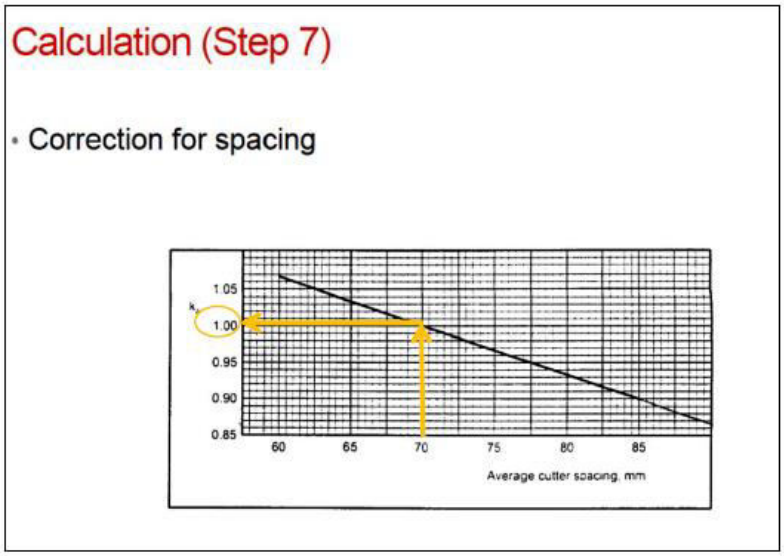

Figure 3.8: correction for spacing Ks.

3.1.7 Step 8:

According to the low porosity hypothesis, K_{por} is equal to 1:

STEP 8	
k_{por} =	1

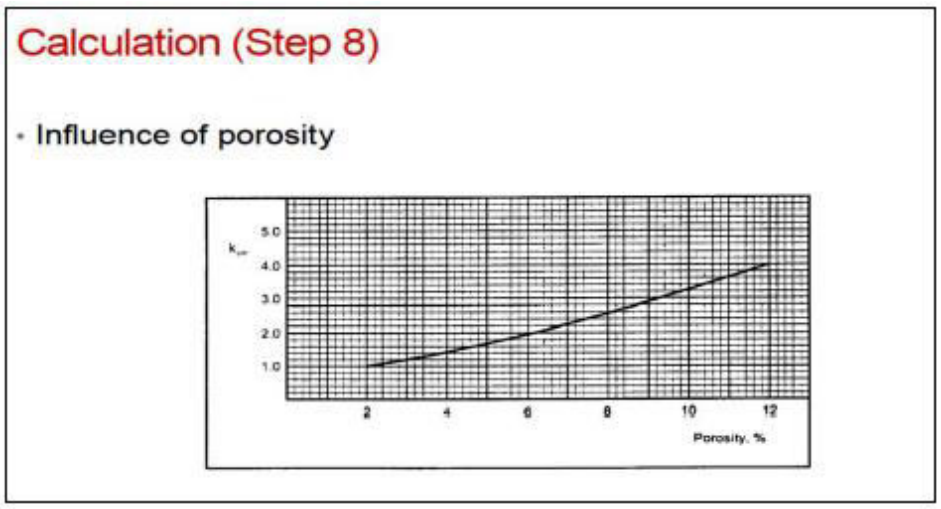

Figure 3.9: calculation of the influence of porosity.

3.1.10 Step 11:

The step 11 is characterized by the calculation of the penetration coefficient B:

K_{ekv}	1,00
B	**1,75**

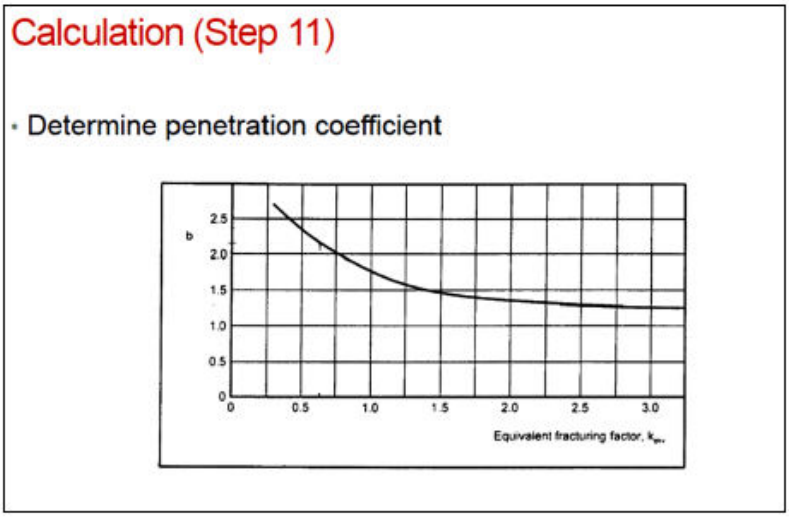

Figure 3.11: penetration coefficient.

3.1.11 Step 12:

The analysis ends with the determination of the base penetration, using the formula:

$$i_0 = \left(\frac{M_{ekv}}{M_1}\right)^b$$

M_{ekv}	259,92
M_1 [KN]	90
B	1,75
i_0 [mm/rev]	**6,40**

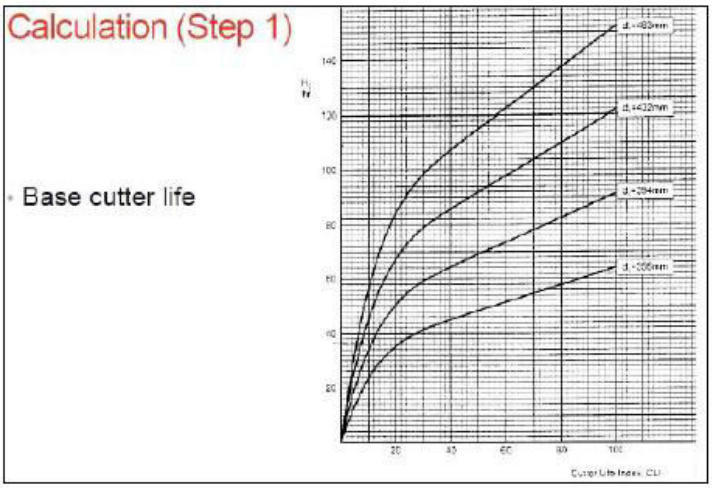

Figure 3.12: graph for the base cutter life.

3.2.2 Step 2

The content of quarzi s the 46.5%, so that correction factor for rock quartz content K_Q is:

Quartz content [%]	46,50
k_Q	**1,01**

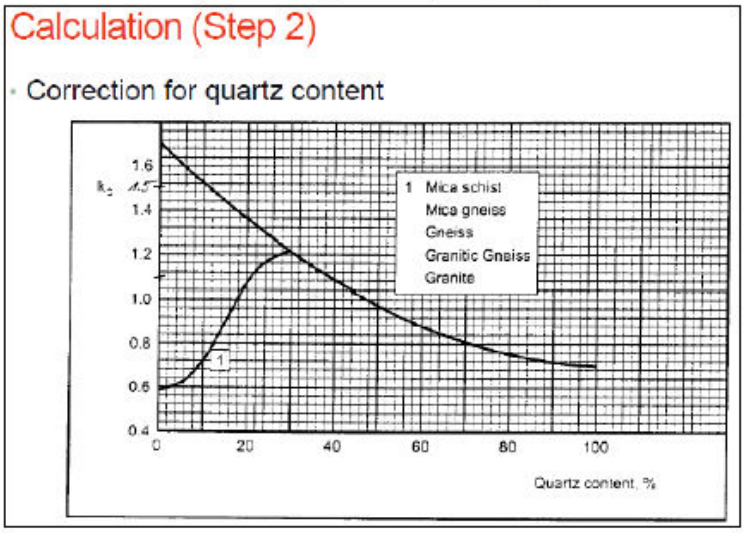

Figure 3.13: correction factor for rock quartz content.

3.2.3 Step 3

Inserting the TBM diameter and interpolating the d_c line, is obtained the RPM. This value is bigger than the design value, so for the calculation of K_{RPM} is used the RPM_{design}.

TBM diameter [m]	4,2
d_c [mm]	431,8
RPM [rev/min]	9
RPM_{DESIGN} [rev/min]	7
K_{RPM}	**1,70**

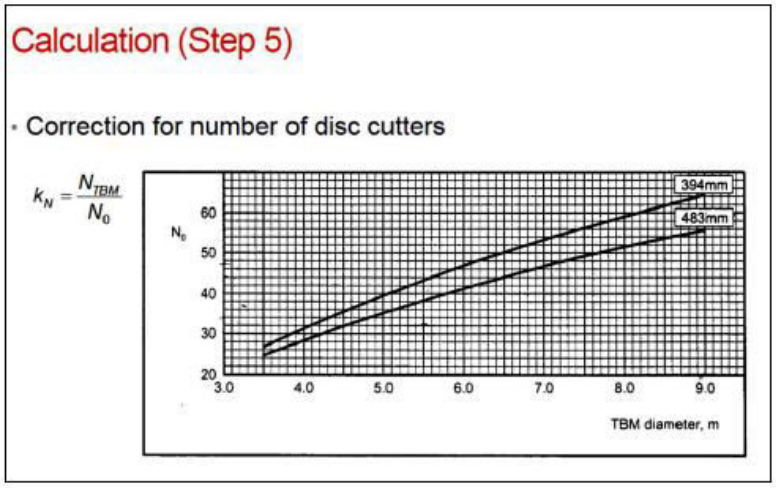

Figure 3.16: correction factor for number of cutters.

3.2.6 Step 6

Using the formula in Figure 3.17 it can be find the cutter life.

H_0	52,00
K_Q	1,01
K_{RPM}	1,70
K_D	1,10
K_n	0,97
N_{TBM}	31,00
H_h [hours/cutter]	**3,07**

D [m]	4,20
i_0 [mm/rev]	6,40
RPM [rev/min]	7
CRL [m^3/cutter]	**114,26**

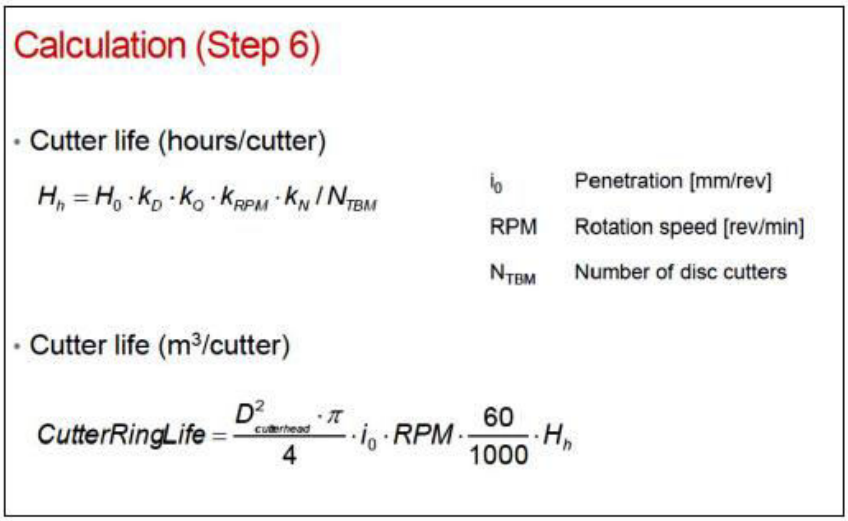

Figure 3.17: cutter life calculation.

4 Ground reinforcing

4.1 Part one

The aim of this exercitation is to analyze a stability problem of a tunnel cross section with a four meter diameter, excavated in conventional method (Drill & Blast technique).
The cross section, as seen in Figure 4.1, is characterized by shale and sandstone; the tunnel has arrived at position AA and some dripping was started, thus the excavation of the tunnel was stopped. So it is necessary to design a ground reinforcing of the area, in order to continue the excavation without problem involving machines and workmen.

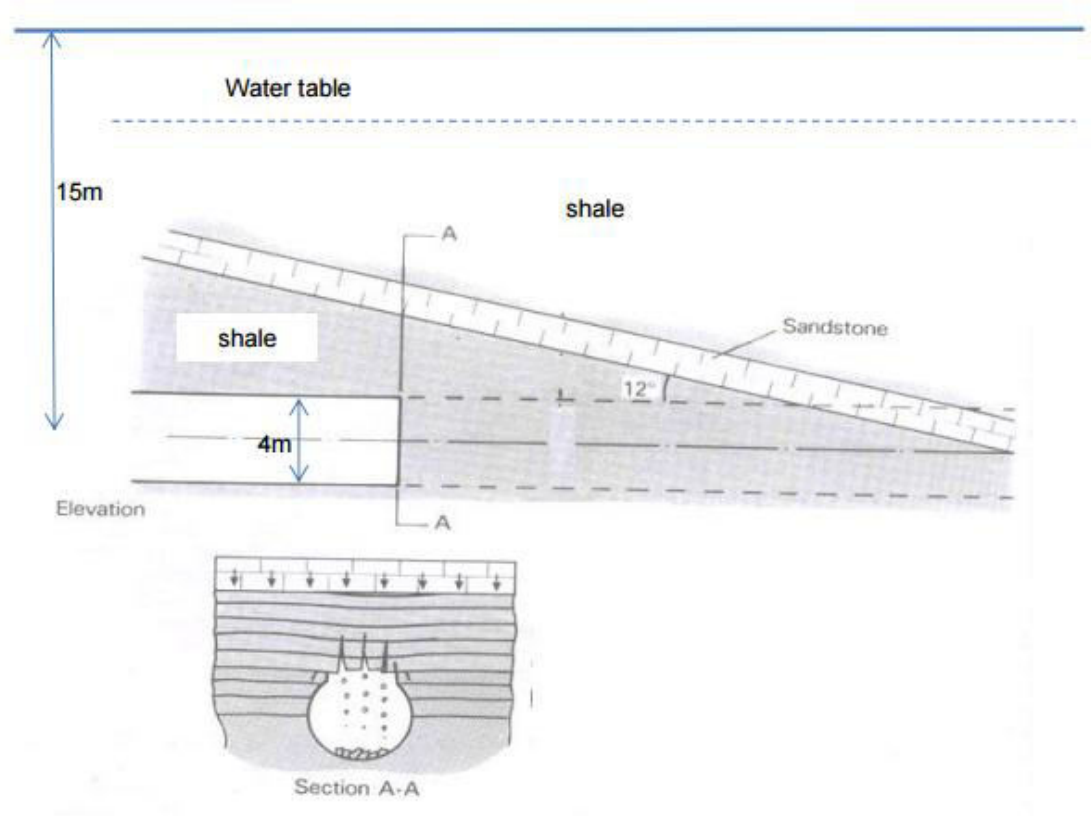

Figure 4.1: cross section.

4.1.1 Preliminary investigation

As explained previously, the ground is composed by Shales and Sandstone:

- Shale is a fine-grained sedimentary rock that forms from the compaction of silt and clay-size mineral particles that we commonly call "mud";
- Sandstone is a sedimentary rock composed of sand-sized grains of mineral, rock or organic material. It also contains a cementing material that binds the sand grains together and may contain a matrix of silt- or clay-size particles that occupy the spaces between the sand grains.

The injections can be done from surface using Manchette pipes and the goal is to create a ring for impermeabilize the tunnel. The phases of design are:

- to define geometry of volume to be treated;
- to choice geometrical patterns;
- to choice type of mix according to the type of rock;
- to define distance between valves of Manchette pipes and to define volume of mix for each valve.

In some favorable geological conditions the stability provided by injections can be enough.

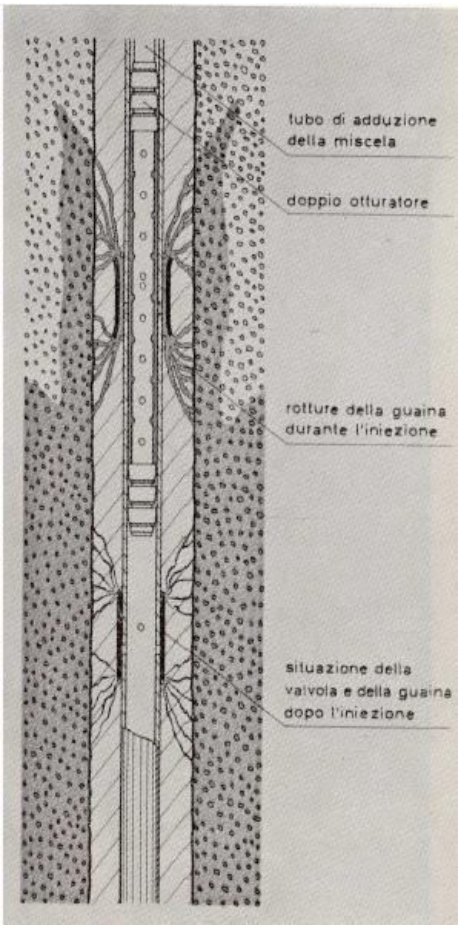

Figure 4.2: Manchette pipe section.

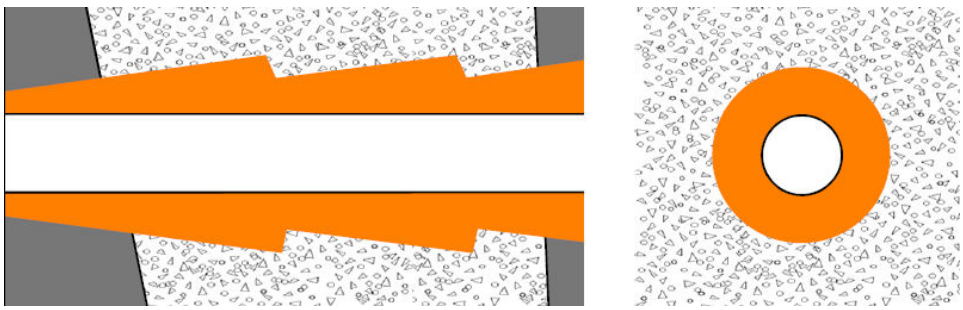

Figure 4.3: injection-grouting section.

This method has advantages and limitations:

- The strength of ground can be increased.
- An impermeable barrier is created.
- It is non-toxic and noiseless.
- It is totally removable (unlike grouting) – although there can be an adverse reaction in some soils.

- The time required to achieve ground freezing can be many weeks depending on the ground and groundwater conditions.
- Flowing water causes heat drain and can prevent the ground freezing. The limiting flow rate depends on the type of freezing being used
- The boreholes must be accurately positioned to create a continuous frozen zone.

4.1.3 Conclusions

Considering the ground characteristics and the different reinforcing methods, forepoling is the best solution because it is possible working safely without dripping and with low costs, unlike freezing which is a very expensive technique and not applicable in a short time.

© Proprietà riservata dell'autore - Digitalizzazione e distribuzione a cura del CENTRO APPUNTI - Corso Luigi Einaudi, 55 - Torino / Pagina 43 di 88

- Evaluate the limit of CPD for the three sections specified on the appended map and verify if the designed round is fulfilling the required CPD.
- Verify if the monitored blasts respect the limits required by the German standard DIN 4150-3 (attached).
- Discuss about the possible problems which can occur and the possible solutions which can be adopted in order to fulfill the requirements of CPD.

5.1 Deisgn blast round of the tunnel

It is necessary sizing the blast with inclined holes opening. Has been designed the blast round of the tunnel by using a V-cut (wedge), including the blasting sequence of each hole.
Once the kind of explosive is chosen and considering that each round must be at least equal of 3 m, using the chart below is possible to extrapolate geometric parameters for the opening blasts.

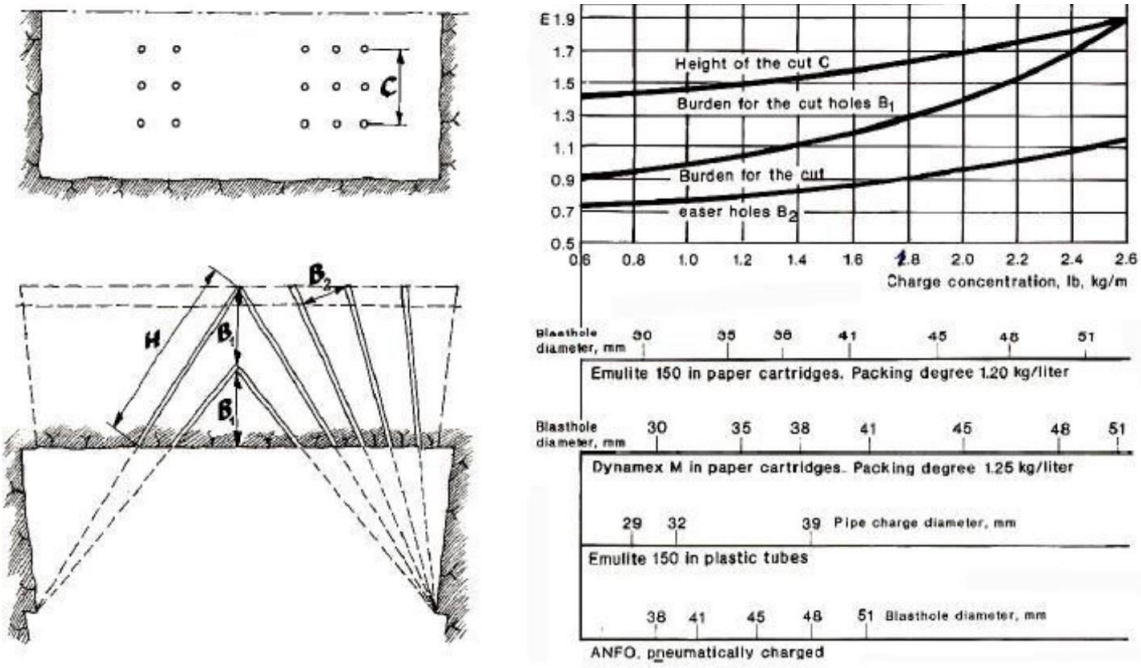

Figure 5.3: charge calculationfor an inclined holes cut.

It was chosen to adopter the explosive *Emulite 150*, that have a charge concentration of 1,20 kg/liter. The following table summarized the data needed for the cut:

Part of the round:	Burden (m)	Spacing (m)	Height bottom charge (m)	Charge concentration Bottom (kg/m)	Charge concentration Column (kg/m)	Stemming (m)
Floor	1×B	1.1×B	1/3×H	l_b	$1.0 \times l_b$	0.2×B
Wall	0.9×B	1.1×B	1/6×H	l_b	$0.4 \times l_b$	0.5×B
Roof	0.9×B	1.1×B	1/6×H	l_b	$0.3 \times l_b$	0.5×B
Stoping:						
Upwards	1×B	1.1×B	1/3×H	l_b	$0.5 \times l_b$	0.5×B
Horizontal	1×B	1.1×B	1/3×H	l_b	$0.5 \times l_b$	0.5×B
Downwards	1×B	1.2×B	1/3×H	l_b	$0.5 \times l_b$	0.5×B

Figure 5.4: production of contour holes.

where the shoulder *B* and the charge concentration l_b can be extracted from the following graphic, coming with the value of the diameter cartridge (38 mm):

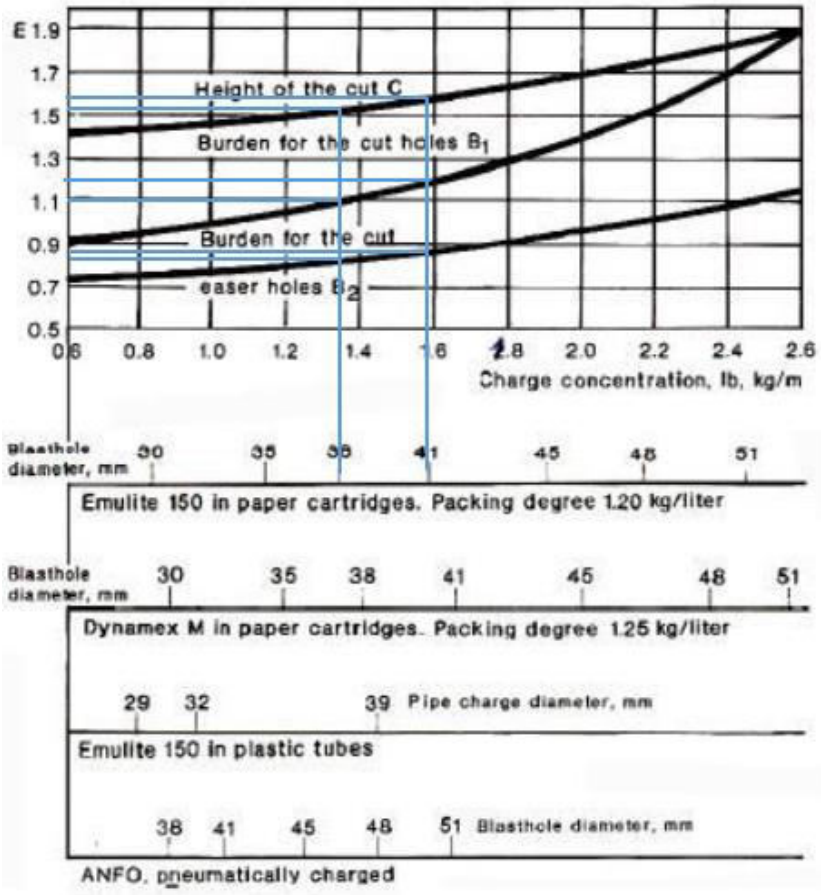

Figure 5.5:the burden B1, B2 and the cut height C in relation to the bottom charge for different blasthole diameters and different explosives.

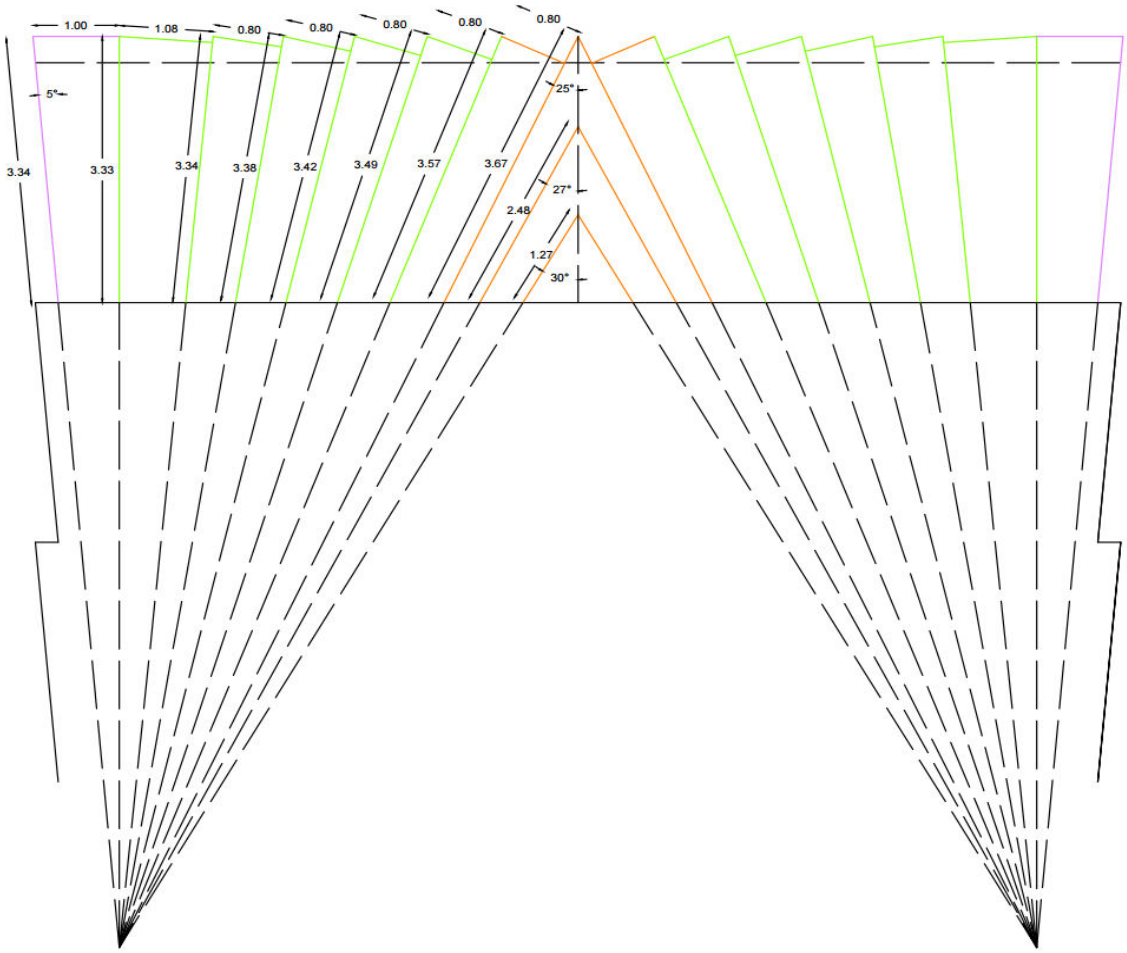

Figure 5.6: v-cut section.

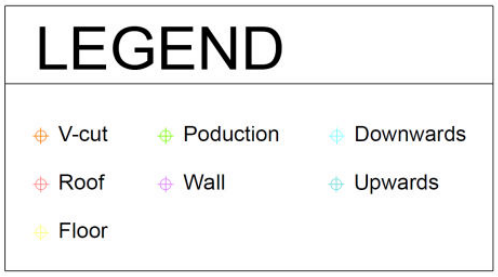

21	857	13,35	15,43	OK
22	874	9,9	15,43	OK
23	891	10,02	15,43	OK
24	908	10,33	15,43	OK
25	925	9,9	15,43	OK
26	942	12,69	15,43	OK
27	959	12,69	15,43	OK
28	976	12,69	15,43	OK
29	993	10,44	15,43	OK

The final time of explosion is equal to **0,993 sec**.

With the data obtained it is possible to calculate the *P.F.* and *S.D.* in order compare them with the theoretical *P.F.* and *S.D.* calculated with the *Mancini and Pelizza's* formula:

$$P.F._{\cdot teorico} \cong \left(\frac{10}{S}0{,}6\right) \cdot A \cdot B \cdot C$$

$$S.D._{\cdot teorico} \cong 2{,}3 \cdot \left(\frac{10}{S}0{,}6\right) \cdot A \cdot B'$$

where the parameters A, B, C, B ' derive from the following table and change on the type of rock, on the explosive and on the blast geometry:

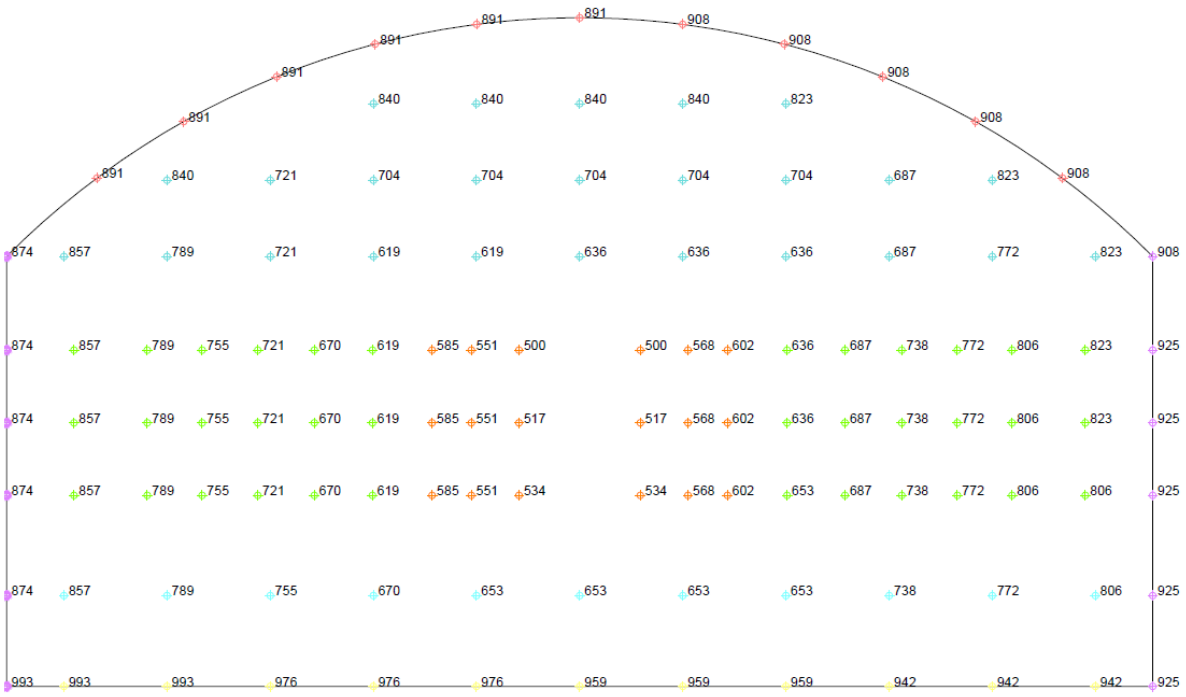

Figure 5.8: firing pattern.

© Proprietà riservata dell'autore - Digitalizzazione e distribuzione a cura del CENTRO APPUNTI - Corso Luigi Einaudi, 55 - Torino / Pagina 53 di 88

6.2 Geotechnical parameters

In order to make a correct design of the tunnel, it is fundamental to assess the typical values for the geotechnical parameters; in more advanced design phases, investigations are unavoidable.
Referring to Figure 1, geomechanical homogenous zones can be distinguished:

- The sand layer extends for 50 m and the ground overburden varies from 2 m to 30 m. It is made by silty sand, whose granulometric curve is represented in Figure 3. The passing percentage at 0.075mm sieve is less than 5%: the fine quantity is very low and, thus, the following geotechnical parameters can be considered:

  - $\gamma = 18\ {}^{KN}/_{m^3}$;
  - $\varphi' = 34°$;
  - $c' = 0\ KPa$;
  - $k_1(30cm) = 30000\ {}^{KN}/_{m^3}$ $(reaction\ coefficient)$;
  - $n = 0{,}25$.

Using a safety factor equal to 1.3, the design values are:

  - $\boldsymbol{\gamma = 18\ {}^{KN}/_{m^3}}$;
  - $\boldsymbol{\varphi' = 27{,}4°}$;
  - $\boldsymbol{c' = 0\ KPa}$;
  - $\boldsymbol{k_1(30cm) = 30000\ {}^{KN}/_{m^3}}$ $\boldsymbol{(reaction\ coefficient)}$;
  - $\boldsymbol{n = 0{,}25}$.

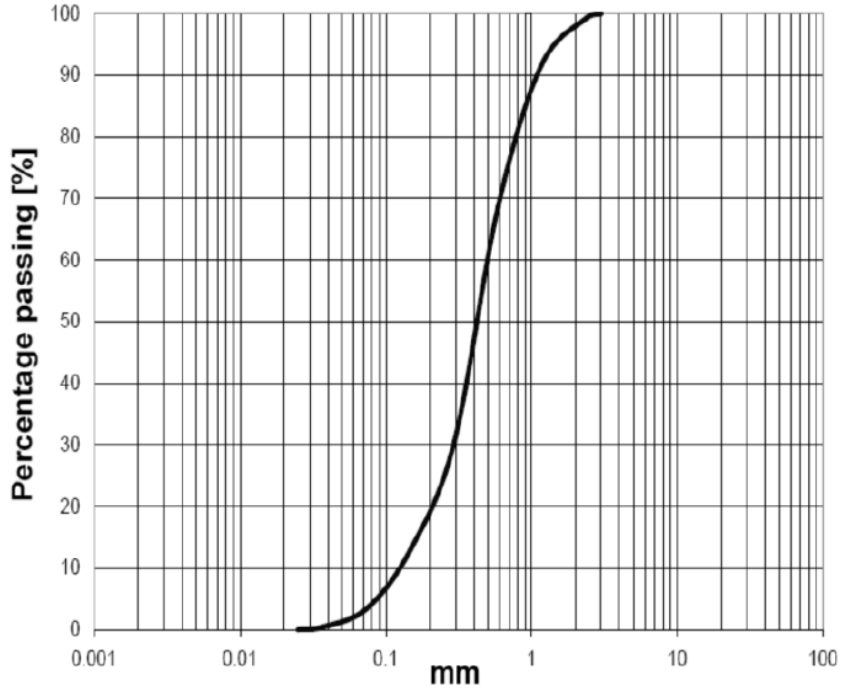

Figure 6.3: sand granulometric curve.

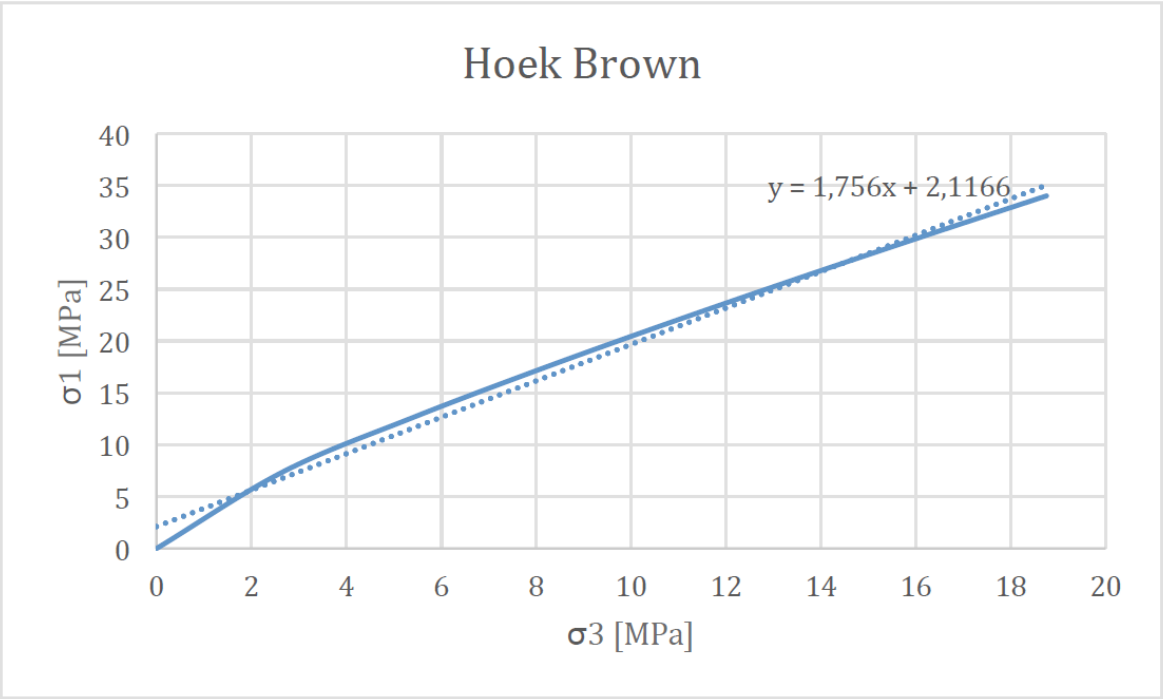

Figure 6.4: Hoek-Brown linearization.

Material	g[$^{KN}/_{m^3}$]	f'	c'[KPa]	E[MPa]	n	$k_1(30cm)$ [$^{KN}/_{m^3}$]
Sand	18	27.4°	0	-	0.25	30000
Morain	18	24°	38.5	3000	0.25	2000000
Fractured limestone	25	12.4°	614	-	-	-

6.3 Excavation in sand layer

To excavate through the sand, the following technologies are considered:

- To obtain an adequate free length and to guarantee the general stability of the tunnel, pre supports ahead the tunnel face are necessary. Jet grouting canopy is the chosen system because the sand is cohesion-less and, thus, it is necessary to construct a continuous support to avoid the material flow. The length of the jet grouting canopy is 15 m and the overlap is 5 m. The inclination of the get grouting canopy is 5° respect to the horizontal direction.
- To assure the face stability, face supports are used: jet grouting longitudinal elements are injected in the soil for a length of 15 m and an overlap of 5 m.
- The excavation is performed by roadheaders which also destroy fiber glass elements.

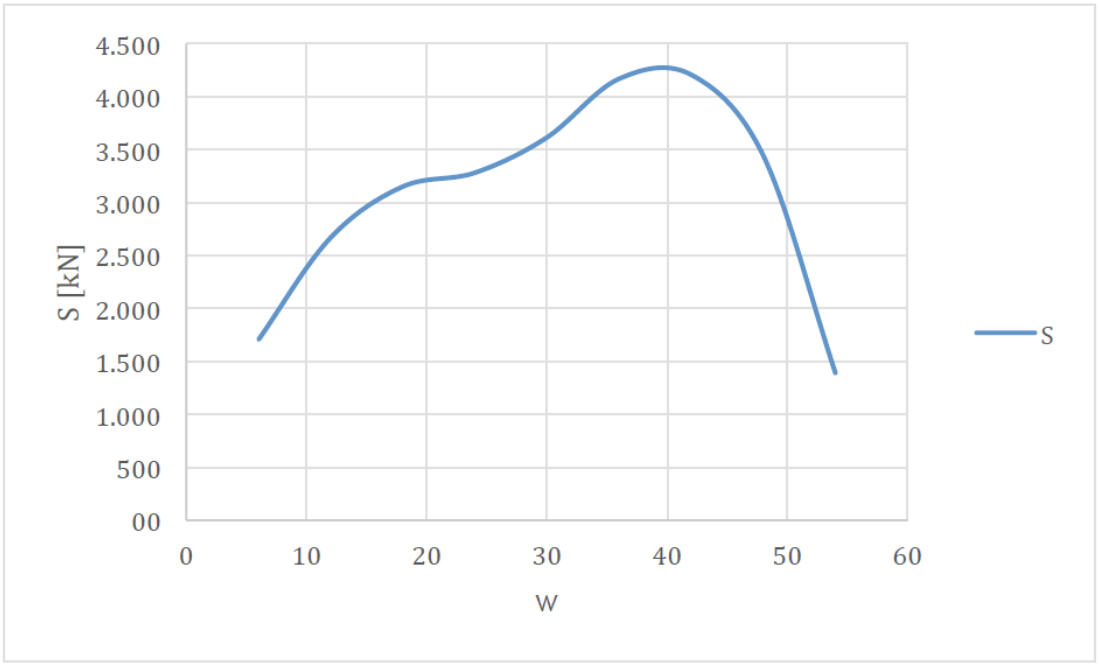

Figure 6.5: Anagnostou method - Face stability.

Because S>0 it is necessary to design a support force $S_{support} > S$ (ω = [0°; 54°]) . Because it is already necessary to use a machine to construct the jet grouting canopy, it has been considered advantageous to use the same machine to create longitudinal jet grouting face supports.
The characteristics of the jet grouting elements are the following:

- Obtained diameter: Φ =70 cm;
- Shear resistance along the surface: considering a compression resistance of the jet grout equal to 10 MPa and using Tresca criteria (figure 6), the shear resistance is equal to: τ=10/2=5 MPa;
- Length: 5 m (this value is the overlapping length, corresponding to the most critical stage of the excavation process);
- 10 jet grout elements drilled, in the vertical direction, each 2 m:
- z=2 m: 3 elements;
- z=4 m: 3 elements;
- z=6 m: 2 elements;
- z=8 m: 2 elements.

w	24			30			36		
z [m]	n elements/row	L [m]	Ss [kN]	n elements/row	L [m]	Ss [kN]	n elements/row	L [m]	Ss [kN]
2	3	0.2	5772.7	3	0.4	5772.7	3	0.6	5772.7
4	3	0.4	5772.7	3	0.9	5772.7	3	1.3	5772.7
6	2	0.6	3848.5	2	1.3	3848.5	2	1.9	3848.5
8	2	0.8	3848.5	2	1.7	3848.5	2	2.6	0
Ss,tot(w) [kN]			19242.3			19242.3			15393.8

w	42			48			54		
z [m]	n elements/row	L [m]	Ss [kN]	n elements/row	L [m]	Ss [kN]	n elements/row	L [m]	Ss [kN]
2	3	0.2	5772.7	3	0.4	5772.7	3	0.6	5772.7
4	3	0.4	5772.7	3	0.9	5772.7	3	1.3	0
6	2	0.6	0	2	1.3	0	2	1.9	0
8	2	0.8	0	2	1.7	0	2	2.6	0
Ss,tot(w) [kN]			11545.4			11545.4			5772.7

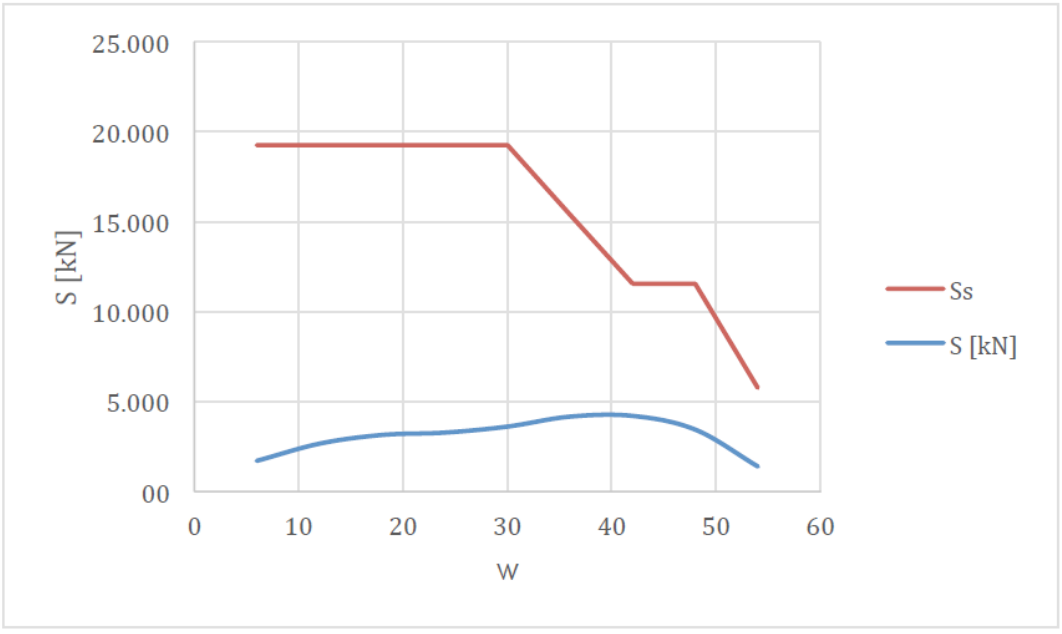

Figure 6.7: Anagnostou method - Face stability.

Observing Figure 6.7, the face supports should appear over-dimensioned. However, a great number of elements were used in order to assure the stability of the entire face, avoiding local collapses. Finally, the jet-grout face support was considered more advantageous than fiberglass elements because the same machine that constructed the jet-grouting arch can be employed. In this case, only 10 jet grout elements have to be added to the 83 elements of the jet-grouting canopy.

- Characteristic jet grout stress resistances: σ_c=10 MPa; σ_t=-3 MPa; design jet grout stress resistances: σ_c=10/1.3=7.7 MPa; σ_t=-3/1.3=-2.3 MPa

Using this pressure, a numerical analysis can be carried out: bedded beam spring method is the used interaction method.
This method allows considering the passive loads applied to the arch, induced by the arch displacement towards the rock. A series of elasto-plastic springs are considered, with a reaction coefficient:

$$k_n = k_1(0.30)\left(\frac{B + 2 * 0.30}{2B}\right)^2 = 30\frac{MN}{m^3}\left(\frac{1 + 2 * 0.30}{2 * 1}\right)^2 = 19.2\frac{MN}{m^3}$$

$$k_t = 0.3k_n = 6.4\frac{MN}{m^3}$$

The software output contains the deformations and the stresses (N, M, T) inside the jet grouting canopy:

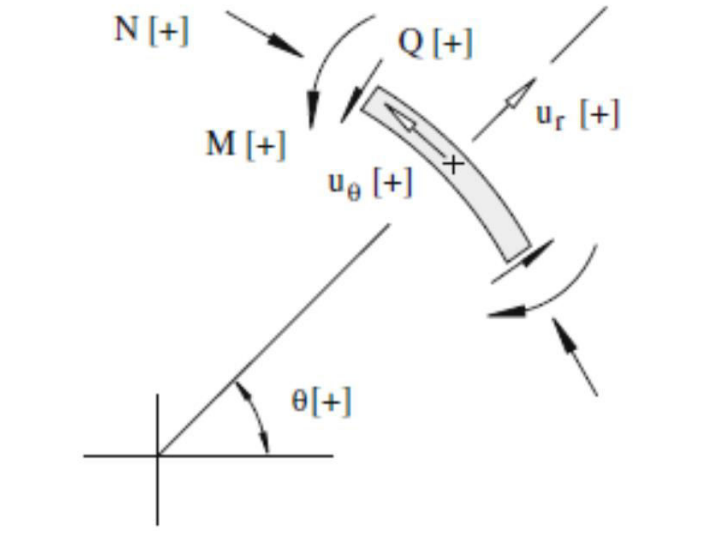

Figure 6.9: displacement and stress conventions

© Proprietà riservata dell'autore - Digitalizzazione e distribuzione a cura del CENTRO APPUNTI - Corso Luigi Einaudi, 55 - Torino / Pagina 63 di 88

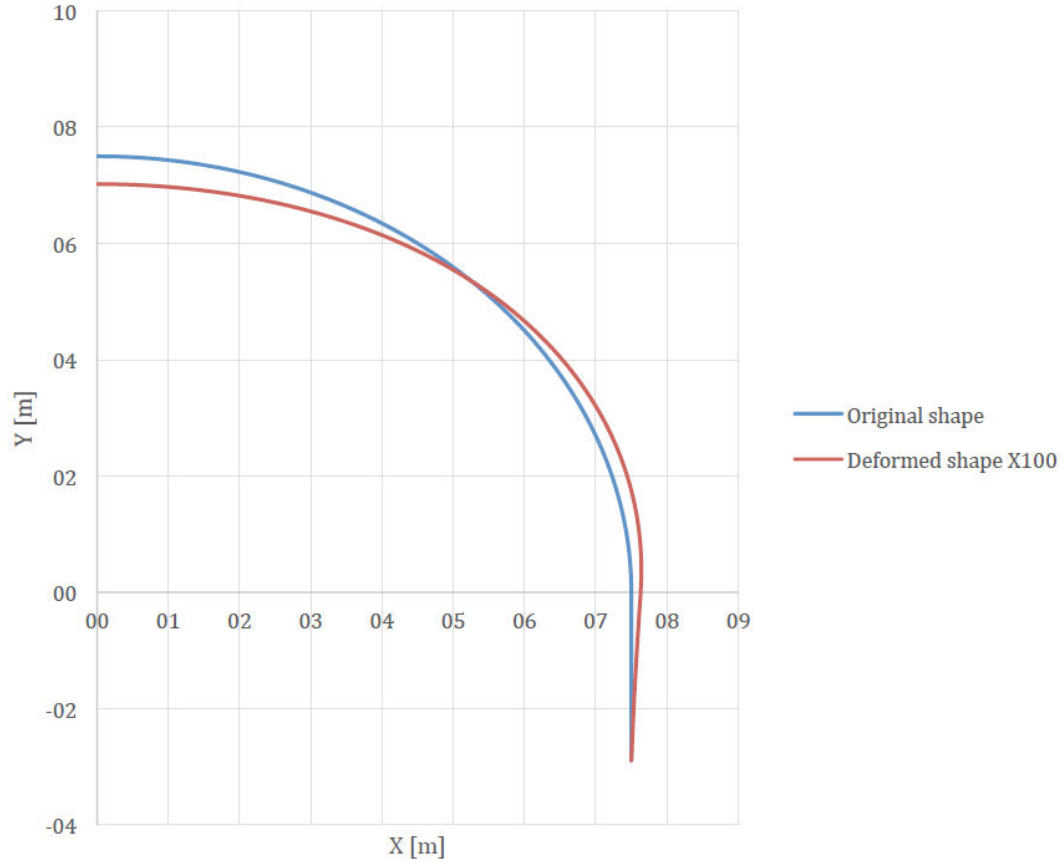

Figure 6.10: deformend shape.

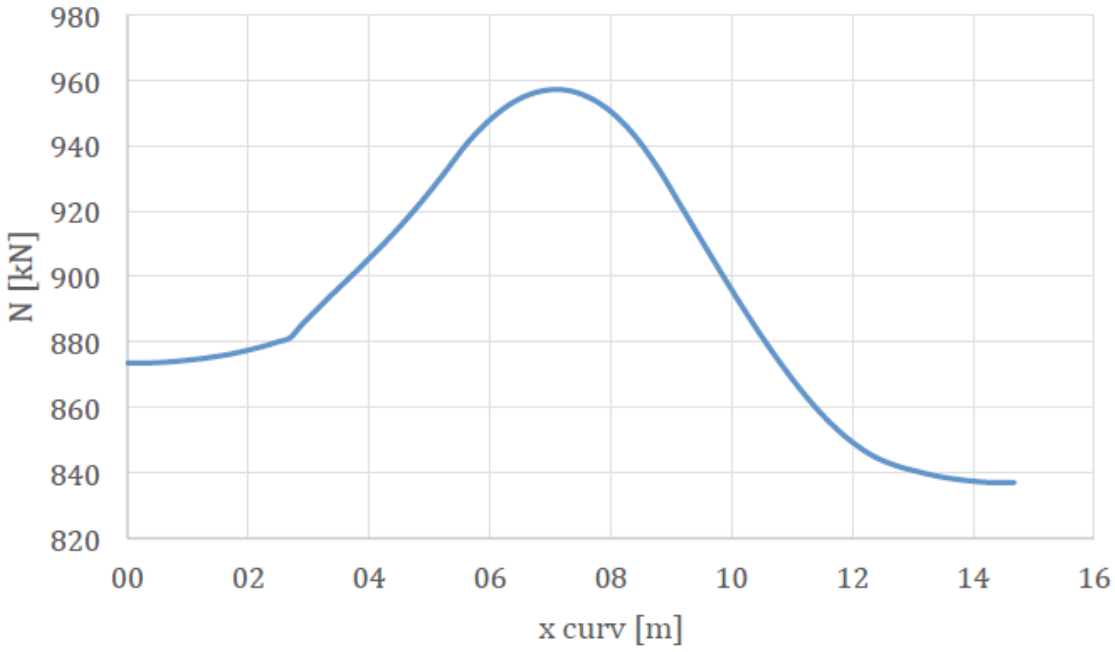

Figure 6.11: normal stress of the cross section.

© Proprietà riservata dell'autore - Digitalizzazione e distribuzione a cura del CENTRO APPUNTI - Corso Luigi Einaudi, 55 - Torino / Pagina 65 di 88

$$\sigma^{\pm} = \frac{N}{A} \pm \frac{M}{W}$$

The interaction between normal force and shear force is carried out considering the following relationships:

$$\begin{cases} \sigma_{max} = \dfrac{N}{A} \\ \tau_{max} = \dfrac{3T}{2A} \ (calculated\ at\ the\ centre\ of\ the\ jet\ grout) \\ \sigma_{1,3} = \dfrac{\sigma_{max}}{2} \pm \sqrt{(\dfrac{\sigma_{max}}{2})^2 + \tau^2{}_{max}} \end{cases}$$

All the calculated stresses (table 4: σ+ -; σ1 3) fulfill the stress limitations.

$$\sigma_t = -2.3MPa \leq \sigma^{\pm} \leq \sigma_c = 7.7\ MPa$$
$$\sigma_t = -2.3MPa \leq \sigma_{1,3} \leq \sigma_c = 2.3\ MPa$$

6.3.3 First phase lining - Sand

First phase lining is constructed using shotcrete:

- Fiber-reinforced concrete (thus, it is not necessary to install the mesh, minimizing the installation operations);
- Thickness: 23 cm (concrete cover: 1.5 cm);
- Steel rib: HEB 200 (thickness: 20 cm; area: 0.007808 m2; inertia: 0.00005696 m4);
- Interax between steel ribs: 1.25 m;
- Concrete properties: Ec=20 GPa; maximum stresses: $\sigma_c^+ = 30\ MPa$; $\sigma_c^- = -4\ MPa$; design maximum stresses: $\sigma_c^+ = 23\ MPa$; $\sigma_c^- = -3.1\ MPa$;
- Steel properties: Ec=210 GPa; maximum stresses: $\sigma_c^+ = 300\ MPa$; $\sigma_c^- = -300\ MPa$; design maximum stresses: $\sigma_c^+ = 231\ MPa$; $\sigma_c^- = -231\ MPa$;
- Mean radius: 7.1 m.
- Equivalent cross section (same axial and bending stiffness of the shotcrete section can be evaluated):

$$h_{eq} = \sqrt{\frac{12(E_c I_c + E_s I_s)}{E_c A_c + E_s A_s}}$$
$$E_{eq} = \frac{E_c A_c + E_s A_s}{B h_{eq}}$$

where:

B is the width considered: 1 m;

© Proprietà riservata dell'autore - Digitalizzazione e distribuzione a cura del CENTRO APPUNTI - Corso Luigi Einaudi, 55 - Torino / Pagina 67 di 88

NODE	X [m]	Y [m]	Curvilineous coordinate [m]	N [kN]	T [kN]	M [kNm]	Nc [kN]	Ns [kN]	Tc [kN]	Ts [kN]	Mc [kNm]	Ms [kNm]
1	7.1	-2.6	0.0	800.7	-69.2	0.0	619.2	181.5	-53.5	-15.7	0.0	0.0
2	7.1	-2.4	0.2	800.8	-69.2	-12.9	619.3	181.5	-53.5	-15.7	-8.6	-4.2
3	7.1	-2.2	0.4	801.0	-59.6	-23.9	619.4	181.6	-46.1	-13.5	-16.0	-7.9
4	7.1	-2.0	0.6	801.3	-49.9	-33.2	619.7	181.6	-38.6	-11.3	-22.2	-11.0
5	7.1	-1.9	0.7	801.7	-40.2	-40.7	620.0	181.7	-31.1	-9.1	-27.2	-13.4
6	7.1	-1.7	0.9	802.2	-30.6	-46.3	620.4	181.8	-23.6	-6.9	-31.0	-15.3
7	7.1	-1.5	1.1	802.8	-20.9	-50.2	620.8	182.0	-16.2	-4.7	-33.6	-16.6
8	7.1	-1.3	1.3	803.5	-11.3	-52.3	621.4	182.1	-8.7	-2.6	-35.0	-17.3
9	7.1	-1.1	1.5	804.3	-1.6	-52.6	622.0	182.3	-1.2	-0.4	-35.2	-17.4
10	7.1	-0.9	1.7	805.3	8.0	-51.1	622.8	182.5	6.2	1.8	-34.2	-16.9
11	7.1	-0.7	1.9	806.3	17.7	-47.8	623.5	182.8	13.7	4.0	-32.0	-15.8
12	7.1	-0.6	2.0	807.4	27.4	-42.7	624.4	183.0	21.2	6.2	-28.6	-14.1
13	7.1	-0.4	2.2	808.6	37.0	-35.9	625.3	183.3	28.6	8.4	-24.0	-11.9
14	7.1	-0.2	2.4	809.9	46.7	-27.2	626.3	183.6	36.1	10.6	-18.2	-9.0
15	7.1	0.0	2.6	812.9	56.3	-16.7	628.6	184.3	43.6	12.8	-11.2	-5.5
16	7.1	0.4	3.0	817.9	49.6	1.7	632.5	185.4	38.4	11.3	1.1	0.6
17	7.1	0.7	3.3	823.2	30.2	12.9	636.6	186.6	23.3	6.8	8.7	4.3
18	7.0	1.1	3.7	830.2	15.7	18.8	642.0	188.2	12.1	3.5	12.5	6.2
19	6.9	1.5	4.1	840.2	5.2	20.7	649.7	190.5	4.0	1.2	13.8	6.8
20	6.9	1.8	4.5	854.1	-1.1	20.3	660.5	193.6	-0.8	-0.2	13.6	6.7
21	6.8	2.2	4.8	868.1	-4.9	18.5	671.3	196.8	-3.8	-1.1	12.4	6.1
22	6.6	2.5	5.2	881.7	-6.2	16.2	681.8	199.9	-4.8	-1.4	10.8	5.4
23	6.5	2.9	5.6	894.7	-5.7	14.1	691.9	202.8	-4.4	-1.3	9.4	4.7
24	6.3	3.2	5.9	906.8	-4.4	12.5	701.2	205.6	-3.4	-1.0	8.3	4.1
25	6.1	3.6	6.3	917.8	-1.7	11.8	709.8	208.0	-1.3	-0.4	7.9	3.9
26	6.0	3.9	6.7	927.6	1.0	12.2	717.3	210.3	0.7	0.2	8.2	4.0
27	5.7	4.2	7.1	935.8	3.9	13.6	723.7	212.1	3.0	0.9	9.1	4.5
28	5.5	4.5	7.4	942.3	6.5	16.1	728.7	213.6	5.1	1.5	10.7	5.3
29	5.3	4.8	7.8	946.6	8.5	19.2	732.0	214.6	6.6	1.9	12.9	6.4
30	5.0	5.0	8.2	948.4	9.7	22.8	733.4	215.0	7.5	2.2	15.3	7.5
31	4.8	5.3	8.5	947.1	8.3	25.9	732.4	214.7	6.4	1.9	17.4	8.6
32	4.5	5.5	8.9	941.9	5.4	27.9	728.4	213.5	4.1	1.2	18.7	9.2
33	4.2	5.7	9.3	933.9	-1.1	27.5	722.2	211.7	-0.9	-0.3	18.4	9.1
34	3.9	6.0	9.7	926.1	-9.5	24.0	716.2	209.9	-7.4	-2.2	16.0	7.9
35	3.6	6.1	10.0	918.8	-15.9	18.0	710.5	208.3	-12.3	-3.6	12.1	6.0
36	3.2	6.3	10.4	912.2	-20.6	10.4	705.4	206.8	-15.9	-4.7	7.0	3.4
37	2.9	6.5	10.8	906.7	-22.9	1.9	701.2	205.5	-17.7	-5.2	1.3	0.6
38	2.5	6.6	11.1	902.3	-24.1	-7.1	697.8	204.5	-18.6	-5.5	-4.7	-2.3
39	2.2	6.8	11.5	899.3	-23.5	-15.8	695.4	203.9	-18.2	-5.3	-10.6	-5.2
40	1.8	6.9	11.9	897.8	-21.7	-23.9	694.3	203.5	-16.8	-4.9	-16.0	-7.9
41	1.5	6.9	12.3	898.1	-19.2	-31.0	694.5	203.6	-14.8	-4.3	-20.8	-10.3
42	1.1	7.0	12.6	900.2	-15.3	-36.7	696.1	204.1	-11.8	-3.5	-24.6	-12.1
43	0.7	7.1	13.0	904.1	-11.3	-40.9	699.2	204.9	-8.7	-2.6	-27.4	-13.5
44	0.4	7.1	13.4	906.1	-6.8	-43.4	700.7	205.4	-5.2	-1.5	-29.0	-14.4
45	0.0	7.1	13.8	906.1	-2.4	-44.3	700.7	205.4	-1.8	-0.5	-29.6	-14.6

© Proprietà riservata dell'autore - Digitalizzazione e distribuzione a cura del CENTRO APPUNTI - Corso Luigi Einaudi, 55 - Torino / Pagina 69 di 88

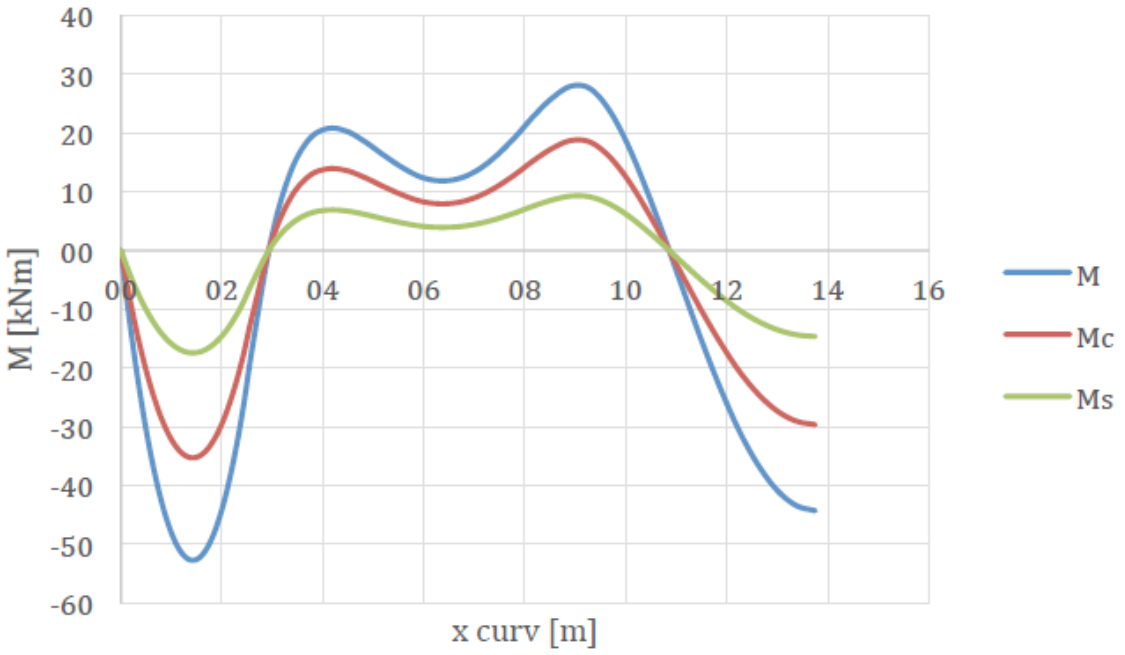

Figure 6.16: bending moment.

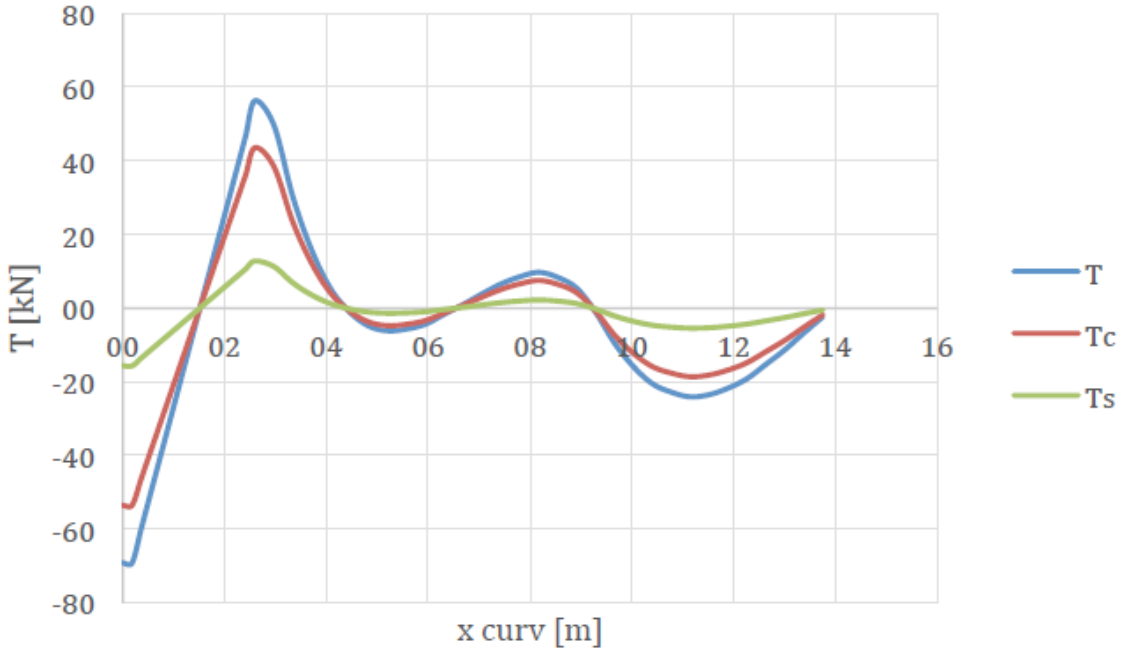

Figure 6.17: shear stress.

© Proprietà riservata dell'autore - Digitalizzazione e distribuzione a cura del CENTRO APPUNTI - Corso Luigi Einaudi, 55 - Torino / Pagina 71 di 88

NODE	X [m]	Y [m]	Curvilineous coordinate [m]	σ c+ [Mpa]	σ c- [Mpa]	σ s+ [Mpa]	σ s- [Mpa]	σ c1 [Mpa]	σ c3 [Mpa]	σ s1 [Mpa]	σ s3 [Mpa]
1	7.1	-2.6	0.0	2.8	2.8	29.1	29.1	2.8	0.0	29.5	-0.5
2	7.1	-2.4	0.2	3.8	1.7	38.4	19.7	2.8	0.0	29.5	-0.5
3	7.1	-2.2	0.4	4.7	0.9	46.4	11.7	2.8	0.0	29.4	-0.4
4	7.1	-2.0	0.6	5.4	0.1	53.2	5.0	2.8	0.0	29.3	-0.3
5	7.1	-1.9	0.7	6.0	-0.5	58.6	-0.4	2.8	0.0	29.3	-0.2
6	7.1	-1.7	0.9	6.5	-0.9	62.7	-4.5	2.8	0.0	29.2	-0.1
7	7.1	-1.5	1.1	6.8	-1.2	65.6	-7.3	2.8	0.0	29.2	0.0
8	7.1	-1.3	1.3	6.9	-1.4	67.1	-8.8	2.8	0.0	29.2	0.0
9	7.1	-1.1	1.5	7.0	-1.4	67.4	-9.0	2.8	0.0	29.2	0.0
10	7.1	-0.9	1.7	6.8	-1.3	66.3	-7.9	2.8	0.0	29.2	0.0
11	7.1	-0.7	1.9	6.6	-1.0	64.0	-5.4	2.8	0.0	29.3	0.0
12	7.1	-0.6	2.0	6.2	-0.6	60.3	-1.7	2.8	0.0	29.4	-0.1
13	7.1	-0.4	2.2	5.6	-0.1	55.4	3.3	2.8	0.0	29.5	-0.1
14	7.1	-0.2	2.4	5.0	0.6	49.1	9.7	2.8	0.0	29.6	-0.2
15	7.1	0.0	2.6	4.1	1.5	41.6	17.4	2.8	0.0	29.8	-0.3
16	7.1	0.4	3.0	3.0	2.7	30.9	28.4	2.8	0.0	29.9	-0.2
17	7.1	0.7	3.3	3.9	1.8	39.3	20.5	2.9	0.0	30.0	-0.1
18	7.0	1.1	3.7	4.4	1.4	43.7	16.5	2.9	0.0	30.2	0.0
19	6.9	1.5	4.1	4.5	1.3	45.5	15.5	2.9	0.0	30.5	0.0
20	6.9	1.8	4.5	4.6	1.3	45.7	16.3	3.0	0.0	31.0	0.0
21	6.8	2.2	4.8	4.5	1.5	44.9	18.1	3.0	0.0	31.5	0.0
22	6.6	2.5	5.2	4.3	1.8	43.8	20.2	3.0	0.0	32.0	0.0
23	6.5	2.9	5.6	4.2	2.0	42.7	22.2	3.1	0.0	32.5	0.0
24	6.3	3.2	5.9	4.1	2.1	41.9	23.9	3.1	0.0	32.9	0.0
25	6.1	3.6	6.3	4.1	2.2	41.9	24.7	3.2	0.0	33.3	0.0
26	6.0	3.9	6.7	4.2	2.2	42.5	24.8	3.2	0.0	33.7	0.0
27	5.7	4.2	7.1	4.3	2.2	43.8	24.1	3.2	0.0	34.0	0.0
28	5.5	4.5	7.4	4.5	2.0	45.9	22.5	3.3	0.0	34.2	0.0
29	5.3	4.8	7.8	4.8	1.7	48.3	20.4	3.3	0.0	34.4	0.0
30	5.0	5.0	8.2	5.1	1.5	51.0	17.8	3.3	0.0	34.4	0.0
31	4.8	5.3	8.5	5.3	1.2	53.2	15.6	3.3	0.0	34.4	0.0
32	4.5	5.5	8.9	5.5	1.0	54.4	13.9	3.3	0.0	34.2	0.0
33	4.2	5.7	9.3	5.4	1.0	53.8	13.9	3.2	0.0	33.9	0.0
34	3.9	6.0	9.7	5.1	1.3	51.0	16.2	3.2	0.0	33.6	0.0
35	3.6	6.1	10.0	4.6	1.7	46.4	20.3	3.2	0.0	33.4	0.0
36	3.2	6.3	10.4	4.0	2.3	40.7	25.6	3.2	0.0	33.1	0.0
37	2.9	6.5	10.8	3.3	3.0	34.3	31.5	3.1	0.0	33.0	0.0
38	2.5	6.6	11.1	3.7	2.6	37.9	27.6	3.1	0.0	32.8	-0.1
39	2.2	6.8	11.5	4.4	1.9	44.1	21.2	3.1	0.0	32.7	-0.1
40	1.8	6.9	11.9	5.0	1.2	49.9	15.3	3.1	0.0	32.6	0.0
41	1.5	6.9	12.3	5.6	0.6	55.1	10.1	3.1	0.0	32.6	0.0
42	1.1	7.0	12.6	6.0	0.2	59.3	6.0	3.1	0.0	32.7	0.0
43	0.7	7.1	13.0	6.4	-0.1	62.5	3.1	3.1	0.0	32.8	0.0
44	0.4	7.1	13.4	6.6	-0.3	64.4	1.4	3.1	0.0	32.9	0.0
45	0.0	7.1	13.8	6.7	-0.4	65.0	0.7	3.1	0.0	32.9	0.0

© Proprietà riservata dell'autore - Digitalizzazione e distribuzione a cura del CENTRO APPUNTI - Corso Luigi Einaudi, 55 - Torino / Pagina 73 di 88

ω [°]	F [m^2]	U [m]	R [m]	σ_v [kPa]	V [kN]	G [kN]	Ts [kN]	S [kN]
6	14.7	30.6	0.5	0.0	0.0	1285.9	388.7	-8351.3
12	29.6	32.7	0.9	0.0	0.0	2600.5	837.8	-6253.2
18	45.3	34.9	1.3	0.0	0.0	3975.2	1353.3	-5136.3
24	62.1	37.3	1.7	0.0	0.0	5447.2	1947.9	-4708.7
30	80.5	39.9	2.0	0.0	0.0	7063.6	2642.7	-4845.1
36	101.3	42.8	2.4	11.7	685.9	8888.9	3470.3	-5123.1
42	125.5	46.2	2.7	29.5	2440.9	11016.0	4481.0	-5700.3
48	154.8	50.3	3.1	47.8	5355.8	13587.8	5756.1	-7061.9
54	191.9	55.4	3.5	67.1	9999.1	16839.4	7432.0	-9740.5
60	241.5	62.4	3.9	87.9	17450.0	21190.9	9757.4	-14726.6
66	313.2	72.4	4.3	110.8	29948.8	27479.2	13233.2	-24090.1
72	429.1	88.6	4.8	136.9	52866.8	37654.1	19036.4	-42866.5
78	655.9	120.3	5.5	167.4	102635.0	57559.0	30716.7	-86682.8
84	1326.5	214.1	6.2	204.4	262406.0	116403.9	66083.3	-235461.6

The face is, thus, stable without the need of face support technologies.

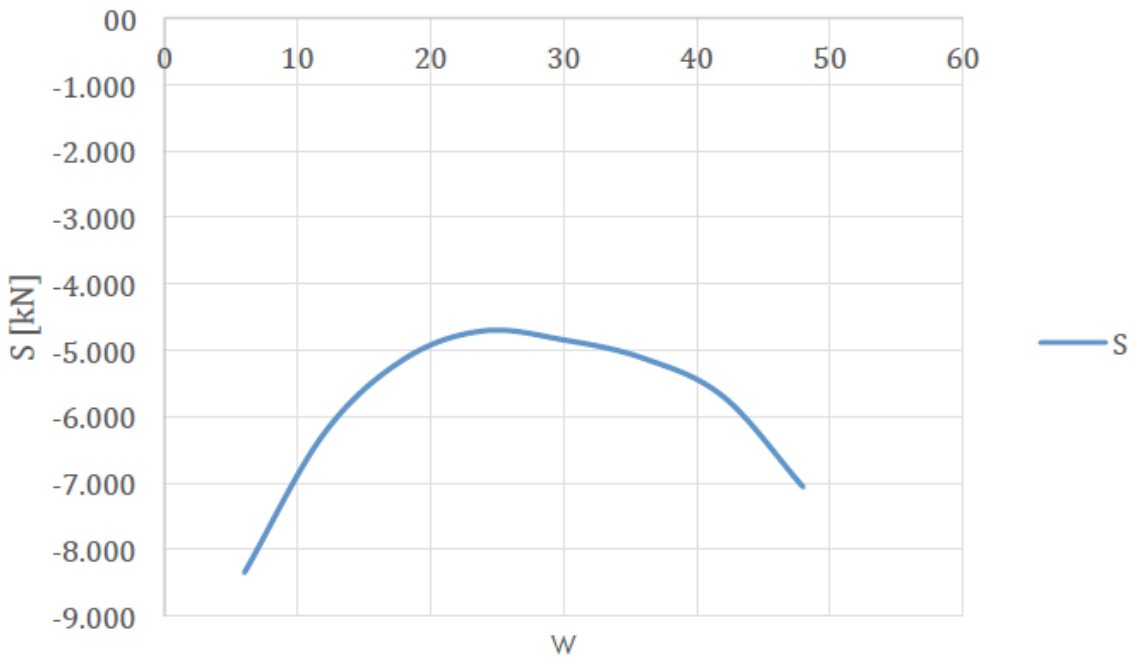

Figure 6.18: Anagnostou method - face stability.

- Interax between steel ribs: 1 m;
- Concrete properties: Ec=20 GPa; maximum stresses: $\sigma_c^+ = 30\ MPa$; $\sigma_c^- = -4\ MPa$; design maximum stresses: $\sigma_c^+ = 23\ MPa$; $\sigma_c^- = -3.1\ MPa$;
- Steel properties: Ec=210 GPa; maximum stresses: $\sigma_c^+ = 300\ MPa$; $\sigma_c^- = -300\ MPa$; design maximum stresses: $\sigma_c^+ = 231\ MPa$; $\sigma_c^- = -231\ MPa$;
- Mean radius: 7.1 m.

Equivalent cross section (same axial and bending stiffness of the shotcrete section can be evaluated):

$$h_{eq} = \sqrt{\frac{12(E_c I_c + E_s I_s)}{E_c A_c + E_s A_s}}$$

$$E_{eq} = \frac{E_c A_c + E_s A_s}{B h_{eq}}$$

where:

B is the width considered: 1 m;

$A_c = BH_c - A_s$;

$I_c = \frac{BH^3{}_c}{12} - \mathrm{I}_s$.

Thus: $h_{eq} = 0.248m;\ E_{eq} = 24.5\ GPa$

The loads transmitted by the soil are evaluated through the Terzaghi formula (multiplied by 40% to consider the benefic front effect):

$$\sigma'_v = 0.4 * 553\ KPa = 260\ KPa$$

The horizontal loads were considered equal to:

$$\sigma'_h = k_a \sigma'_v = \frac{1 - sin\varphi'}{1 + sin\varphi'} \sigma'_v = 0.42 * 260KPa = 110KPa$$

Using this pressure, a numerical analysis can be carried out: bedded beam spring method is the used interaction method. A series of elasto-plastic springs are considered, with a reaction coefficient:

$$k_n = k_1(0.30)\left(\frac{B + 2 * 0.30}{2B}\right)^2 = 200\frac{MN}{m^3}\left(\frac{1 + 2 * 0.30}{2 * 1}\right)^2 = 128\frac{MN}{m^3}$$

$$k_t = 0.3k_n = 42.7\frac{MN}{m^3}$$

Numerical analysis can be performed (software LINING): the software output contains the deformations and the stresses (N, M, T) in the lining:

© Proprietà riservata dell'autore - Digitalizzazione e distribuzione a cura del CENTRO APPUNTI - Corso Luigi Einaudi, 55 - Torino / Pagina 77 di 88

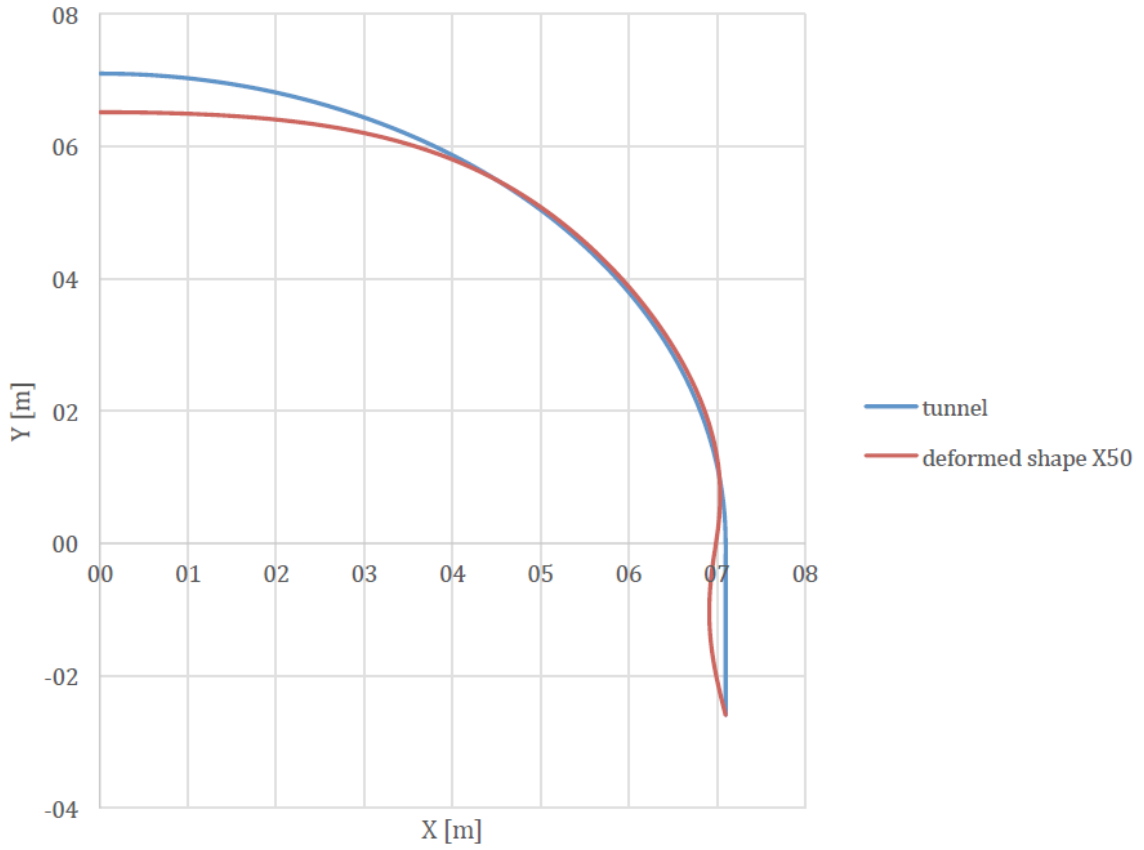

Figure 6.19: deformed mesh.

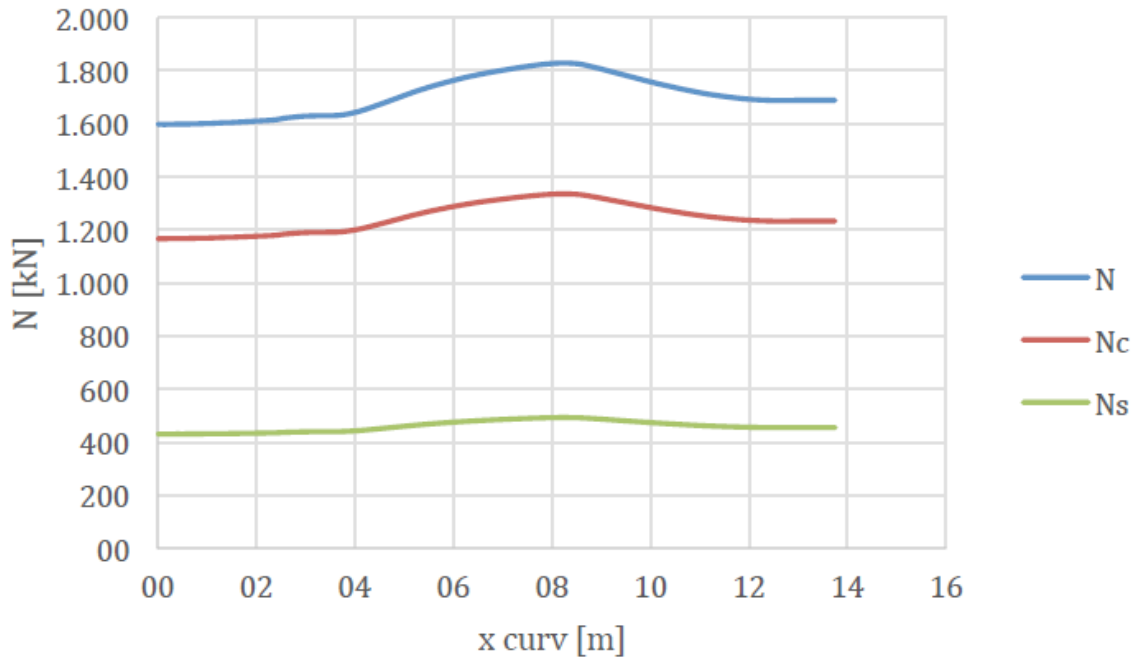

Figure 6.20: normal stress.

Stresses N, M, T have to be distributed between concrete and steel, in function of their stiffness:

$$N_c = N\frac{E_cA_c}{E_cA_c + E_sA_s}$$
$$N_s = N\frac{E_sA_s}{E_cA_c + E_sA_s}$$
$$M_c = M\frac{E_cI_c}{E_cI_c + E_sI_s}$$
$$M_s = M\frac{E_sI_s}{E_cI_c + E_sI_s}$$
$$T_c = T\frac{E_cI_c}{E_cI_c + E_sI_s}$$
$$T_s = T\frac{E_sI_s}{E_cI_c + E_sI_s}$$

The interaction between normal force and bending moment (using a linear elastic theory, with conservation of plane sections) is carried out considering the following relationship:

$$\sigma^{\pm} = \frac{N}{A} \pm \frac{M}{W}$$

The interaction between normal force and shear force is carried out considering the following relationships:

$$\begin{cases} \sigma_{max} = \dfrac{N}{A} \\ \tau_{max} = \dfrac{3T}{2A}\ (calculated\ at\ the\ centre\ of\ the\ jet\ grout) \\ \sigma_{1,3} = \dfrac{\sigma_{max}}{2} \pm \sqrt{(\dfrac{\sigma_{max}}{2})^2 + \tau^2{}_{max}} \end{cases}$$

The described procedure has to be carried out twice, both for concrete, both for shotcrete. The results are, thus: $\sigma_c{}^{\pm}$; $\sigma_s{}^{\pm}$; $\sigma_{1,3.c}$; $\sigma_{1,3.s}$.

© Proprietà riservata dell'autore - Digitalizzazione e distribuzione a cura del CENTRO APPUNTI - Corso Luigi Einaudi, 55 - Torino / Pagina 81 di 88

All the calculated stresses (table 6: $\sigma_c^{\pm}$; $\sigma_s^{\pm}$; $\sigma_{1,3.c}$; $\sigma_{1,3.s}$.) fulfill the stress limitations.

$$\sigma_t = -3.1MPa \leq \sigma_c^{\pm} \leq \sigma_c = 23\ MPa$$
$$\sigma_t = -3.1MPa \leq \sigma_{1,3.c} \leq \sigma_c = 23\ MPa$$
$$\sigma_t = -231MPa \leq \sigma_s^{\pm} \leq \sigma_s = 231\ MPa$$
$$\sigma_t = -231MPa \leq \sigma_{1,3.s} \leq \sigma_s = 231\ MPa$$

6.5 Interventions to cross the contact (fractured limestone)

To allow an adequate free span, a steel pipe umbrella is necessary; in particular the same steel pipes used in the moraine (**DSI ALWAG AT – 168**) are employed.
A special consideration has to be carried out to cross the contact between moraine and limestone, considering the stability of the moraine wedge. Because the dip of the contact is 60°, the thickness of the wedge is equal to: $Htan(90° - dip) = 9.8\tan(30°) = 5.7m$. In order to permit safe working conditions, avoiding the sliding of the wedge, a 2 m extra-length is considered; thus, the total thickness of the wedge is equal to 7.7 m.
A special design of the steel pipe umbrella has to be carried out (see graphical drawings), in order to anchor the steel pipes in the limestone and to cancel vertical loads acting on the wedge.
The wedge can be excavated in a unique phase, by drill and blast, in order to avoid every possible sliding.

si deve rilevare che nel fronte di Cravasco vi è la presenza di Serpentiniti sempre verdi (Amianto) con relativo adeguamento delle metodologie di scavo.

- Illustrazione della geometria dei cantieri:
  si osserva come, da Allegato 1, esistano più fronti di avanzamento con diverse metodologie di scavo dipendenti dalla tipologia del materiale da rimuovere.

  si deve rilevare che alcuni di questi fronti fanno parte del progetto iniziale, mentre altri servono per ridurre i tempi di accesso a questi ultimi.

- Illustrazione delle metodologie di abbattimento
  si osserva che nei due fronti visitati sono stati utilizzati come macchinari di abbattimento una TBM-EPB (Herrekhnect) ed un martello HEIH;

  si deve rilevare che la TBM-EPB è stata utilizzata per accedere al camerone da cui passerà poi la futura tratta.

2. Vista ai cantieri:

- Polcevera:
  Si osserva che dopo il primo tratto scavato con la TBM-EPB, si è realizzato un camerone impermeabilizzato e rivestito con casseformi dal quale verranno realizzati i successivi quattro fronti per due direzioni di marcia.

  Si deve rilevare che la testa della TBM è stata lasciata per questioni economiche in prossimità del camerone; inoltre nella zona antistante il tunnel di accesso sono state realizzate delle vasche per lo smaltimento dello smarino. È stato realizzato uno sbancamento del pendio sovrastante per il posizionamento del gruppo elettrogeno.

- Fegino:
  Si osserva che nel punto di accesso sono state realizzate delle grandi opere di stabilizzazione per ridurre al minimo i cedimenti di alcune strutture posizionate a pochi metri al di sopra dal fronte di scavo. Si sottolinea come questo fronte sia stato scavato interamente con il metodo tradizionale.

© Proprietà riservata dell'autore - Digitalizzazione e distribuzione a cura del CENTRO APPUNTI - Corso Luigi Einaudi, 55 - Torino / Pagina 85 di 88

Allegato 2: documentazione fotografica

Figura 1: Testa della TBM murata all'interno del tunnel dopo alcuni ragionamenti dal punto di vista economico.

Figura 2: cassaforma mobile utilizzata per il final lining

Figura 3: jumbo multibraccio.

Figura 4: impermeabilizzazione a doppia saldatura termica.